The role of specific structural motifs in mode of action of antimicrobial peptide TSO8 from Taenia solium

Begić, Anamarija

University of Split
Faculty of Science

The role of specific structural motifs in mode of action of antimicrobial peptide TSO8 from *Taenia solium*

Master thesis

Anamarija Begić

Split, April 2024.

Temeljna dokumentacijska kartica

Sveučilište u Splitu
Prirodoslovno-matematički fakultet
Odjel za fiziku
Ruđera Boškovića 33, 21000 Split, Hrvatska

Diplomski rad

Uloga specifičnih strukturnih motiva u načinu djelovanja antimikrobnog peptida TSO8 iz *Taenia solium*

Anamarija Begić

Sveučilišni diplomski studij Fizika; smjer: Biofizika

Sažetak:
Borba protiv antimikrobne rezistencije jedan je od glavnih izazova posljednjih desetljeća, potičući potragu za inovativnim liječenjima. Antimikrobni peptidi pojavili su se kao obećavajuća alternativa, obzirom na njihovu važnu ulogu u obrambenom mehanizmu raznih organizama. U ovom radu istražuje se peptid TSO8 identificiran u helmintskom parazitu *Taenia solium,* koji ima značajnu antimikrobnu aktivnost protiv Gram pozitivnih i Gram negativnih bakterijskih sojeva. Detalji mehanizma su istraženi simulacijama molekularne dinamike TSO8 peptida, četiri njegova fragmenta i njegova linearnog oblika, u različitim okruženjima. Rezultati simulacija otkrivaju važnost početnog GW slijeda aminokiselina u stabilizaciji α-helikalne strukture. U interakciji peptida s bakterijskom membranom ističu se dva različita doprinosa: N-terminalna α-uzvojnica ključna je za početni elektrostatski kontakt, dok je funkcija neuređenog C-terminala vjerojatno istaknuta u drugim aspektima aktivnosti peptida. Također, peptidi pokazuju visoku sklonost formiranju klastera u vodi, dok ne pokazuju značajno klasteriranje na površini membrane. U nastavku istraživanja rezultati simulacija će se upotpuniti eksperimentima za biološku i biofizičku karakterizaciju TSO8 peptida i njegovih fragmenata.

Ključne riječi: antimikrobni peptidi, molekularna dinamika, asocijacije, mehanizam djelovanja

Rad sadrži: 61 stranica, 51 slika, 9 tablica, 58 literaturnih navoda. Izvornik je na engleskom jeziku

Mentor: izv. prof. dr. sc. Larisa Zoranić

Ocjenjivači: izv. prof. dr. sc. Larisa Zoranić
doc. dr. sc. Tomislav Rončević
doc. dr. sc. Lucija Krce

Rad prihvaćen: 11. travnja 2024.
Rad je pohranjen u knjižnici Prirodoslovno-matematičkog fakulteta, Sveučilišta u Splitu.

Basic documentation card

University of Split
Faculty of Science
Department of Physics
Ruđera Boškovića 33, 21000 Split, Croatia

Master thesis

The role of specific structural motifs in mode of action of antimicrobial peptide TSO8 from *Taenia solium*

Anamarija Begić

University graduate study Physics, specialization in Biophysics

Abstract:
Combating antimicrobial resistance remains a major challenge in the recent decades, driving the search for innovative treatments. Antimicrobial peptides have emerged as a promising alternative, given their important role in defence mechanism of various organisms. This thesis focuses on TSO8 peptide identified in the helminth parasite *Taenia solium*, which is potent against both Gram-negative and Gram-positive bacterial strains. To assess the atomic details of its mode of action, TSO8 and four of its fragments, along with its linearized form, were investigated through all-atom molecular dynamics simulations in various environments. Results of the simulations reveal the significance of the initial GW amino acid sequence in stabilizing the α-helical structure. In interaction with the bacterial membrane model, two distinct contributions of peptide regions are observed: the N-terminal α-helix is crucial for the initial electrostatic contact, while the function of the unstructured C-terminal is most likely emphasized in other aspects of the peptide's activity. Additionally, peptides show a high affinity of clustering in water, while exhibiting no significant clustering on the membrane surface. For further investigation the insight of MD simulations will be coupled with the biological and biophysical characterization on TSO8 and its fragments.

Keywords: antimicrobial peptides, molecular dynamics, associations, mode of action

Thesis consists of: 61 pages, 51 figures, 9 tables, 58 references. Original language: English

Supervisor: Assoc. Prof. Dr. Larisa Zoranić

Reviewers: Assoc. Prof. Dr. Larisa Zoranić
Assist. Prof. Dr. Tomislav Rončević
Assist. Prof. Dr. Lucija Krce

Thesis accepted: April 11, 2024.
Thesis is deposited in the library of the Faculty of Science, University of Split.

ACKNOWLEDGEMENTS

First and foremost, I would like to thank my mentor Assoc. Prof. Dr. Larisa Zoranić, for guiding me not only in the writing of this thesis but also through my entire academic journey. The support and patience you have shown me, both in academic and personal growth, have been invaluable. Thank you for all the time and effort you keep investing in me!

I am extremely grateful for having the opportunity to learn from Dr. Matko Maleš, who selflessly shared all his knowledge with me, along with his scripts, that saved me so much time and trouble. Thank you for all your help and, very much needed, words of encouragement.

I would also like to thank the reviewers of my thesis, Assist. Prof. Dr. Tomislav Rončević, Assist. Prof. Dr. Lucija Krce and Assist. Prof. Dr. Željka Sanader Maršić for dedicating their time to read my work and for their supportive and kind feedback.

I express my gratitude to the Centre for Advanced Computing and Modelling at the University of Rijeka, for granting me access to their supercomputer "Bura".

Above all, I am thankful to my family and friends for their patience and understanding through all the ups and downs of this chapter of my life.

And finally, to my fiancé, Mirko, who keeps going above and beyond, even learning about the topics outside of his interests, to always help me find solutions to the problems I face. Thank you for being the absolute best "tech support" I somehow always end up needing. None of my achievements would have been possible without your unconditional support and your never-ending belief in me. You are my greatest inspiration!

Contents

1 Introduction

Since the begging of human history, infectious diseases have posed a threat to mankind. A number of devastating bacteria caused epidemics and pandemics, including the Plague of Athens (5th century BC), the Antonine Plague (2nd century), the Plague of Justinian (6th century) and the Black Plague (14th century) led to the decline of cities and even nations [1]. Even though the use of antibiotics dates all the way back to ancient Greece, Egypt, China, and the Roman empire, they have been widely and solely used as the defence against infectious diseases for the past century, since the revolutionary discovery of penicillin by Sir Alexander Fleming in 1928 [2-4]. However, shortly thereafter resistance started to emerge leading to the discovery and development of numerous novel antibiotics during the golden age. Unfortunately, resistance have been reported to nearly all of them, and with the pipeline being exhausted for the past decades, bacterial infections have once again become a great threat [2-4]. In this environment, research into non-conventional antimicrobial agents has intensified, with a few possible candidates being identified, among which are antimicrobial peptides (AMPs) [5, 6].

AMPs are described as multifunctional effector molecules, often gene encoded, produced by almost all organisms (see Figure 1) in which they play a crucial role in the innate non-specific defence system [4]. Their presence all along the evolutionary scale shows their effectiveness and significance on combating invading pathogens like fungi, bacteria, enveloped viruses, and parasites [7].

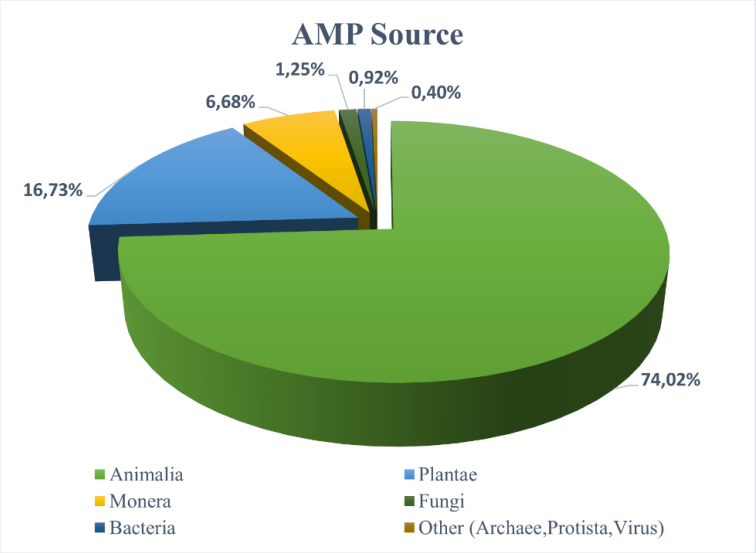

Figure 1 Distribution of natural AMP sources based on sequences in the CAMP$_{R4}$ database. [8, 9]

AMPs are quite short molecules, consisting usually of 10-100 amino acids, with the majority of them being shorter than 50 amino acids (see Figure 2). The net charge of different AMPs varies from -6 to +16, but most of them are cationic with the net charge of about +6. Their cationic nature is crucial for the initial contact with the negatively charged external leaflet of the outer membrane and is reported to be important for their selectivity.

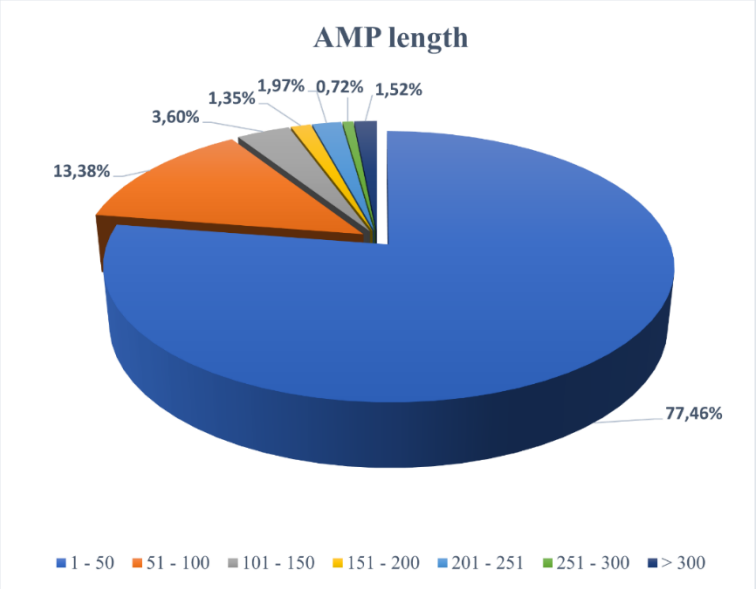

Figure 2 Distribution of AMPs with respect to their number of amino acid residues based on sequences in the $CAMP_{R4}$ database. [8, 9]

AMPs may have different secondary structure conformations, mostly α-helical, linear, β-sheet or hairpin like structures. They carry on average 40-50% of hydrophobic residues arranged so that the folded peptide adopts an amphipathic structure. Amphipathicity, or the formation of topologically distinct hydrophobic and polar regions, is an extremely important property of AMPs, and is crucial in designing new AMPs. Helicity is also reported to play an important role in AMP activity, as well as AMP length and solubility [10-14].

Several modes of action are proposed for AMPs (Figure 3), but can be generally classified into two [14-16]:

1. Direct membrane activity by forming a barrel-like (alamethicin and pardaxin) or toroidal (magainin 2, melittin) pore or by breaking down the membrane into small areas induced by accumulation of peptides on the surface (LL-37).
2. Translocation trough the membrane into the cell where AMPs inhibit vital intercellular processes such as biosynthesis (Bac7), protein folding (pyrrhocoricin), cell wall biosynthesis (human β-defensin), cell division (CRAMP), etc.

It can be said that AMPs interact with the membrane via a two-state model [15]:

1. Binding of the peptide due to electrostatic and then hydrophobic interactions with the membrane lipids.
2. Creation of the above-mentioned defects in the membrane, which can only be achieved if the peptide to lipid ratio is high enough.

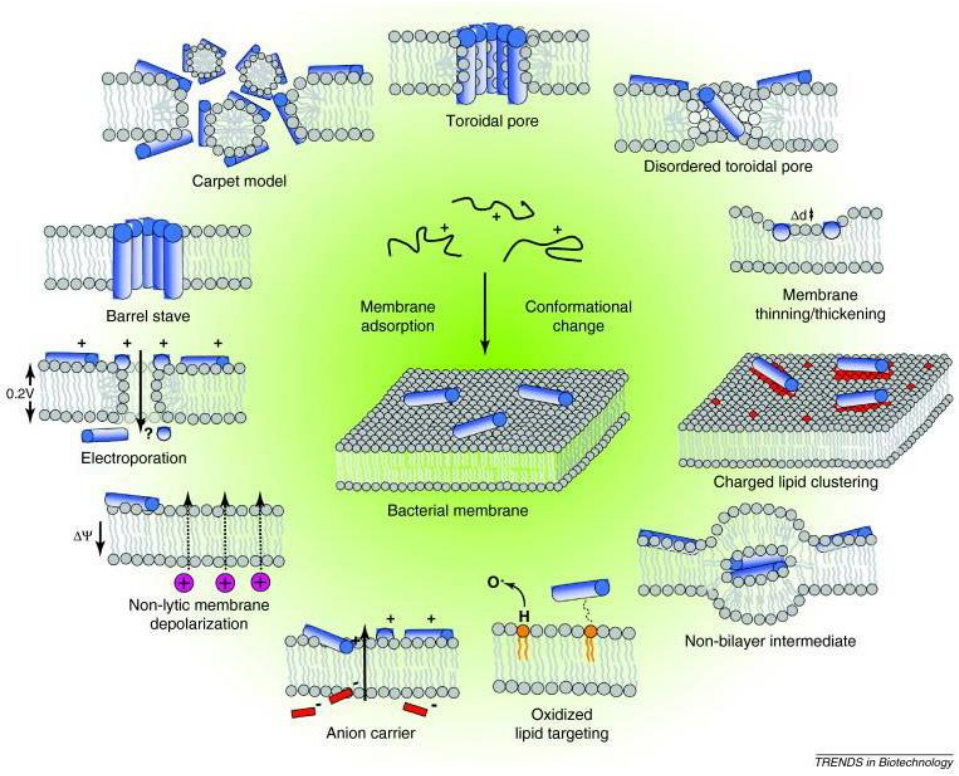

Figure 3 Proposed modes of action of AMPs. Figure taken from Nguyen et al. [14]

Research into AMPs employs various methods to provide insights into their structure, function, and potential applications. Computational modelling stands as a fundamental approach in predicting peptide structures, their interactions with the cell membrane and potential mechanisms of action, using computational algorithms and molecular dynamics (MD) [15, 17]. Circular dichroism (CD) spectroscopy is one of the most widely employed technique for estimating secondary structure of peptides and their conformational changes [11, 18]. Additionally, standard nuclear magnetic resonance (NMR) spectroscopy is used to determine high-resolution structures in aqueous solutions or detergent micelles, while solid-state NMR enables investigation of peptide orientation in lipid bilayers [19]. Complementing these biophysical approaches are biochemical assays, which include minimal inhibitory concentration (MIC) and minimal bactericidal concentration (MBC) determinations. These assays provide crucial information for evaluating the potency, spectrum of activity and potential therapeutic applications of AMPs [11, 18]. Furthermore, peptide synthesis methods, including solid-phase peptide synthesis and recombinant protein expression, facilitate the production of peptide variants with altered sequences or post-translational modifications to enhance their antimicrobial properties or pharmacokinetic profiles [10]. By integrating these biophysical, biochemical, computational, and molecular biology approaches, researchers can gain a comprehensive understanding of AMPs structure, function, and therapeutic potential, paving the way for the development of next-generation antimicrobial agents to combat drug-resistant infections.

In this thesis, computational methods of molecular dynamic simulations were employed to investigate the structural stability and potential mode of action of an antimicrobial peptide from a helminth parasite. Due to their limited representation among all identified AMPs, those

originating from helminth parasites are often overlooked in drug development discussions. Parasitism is recognized as a successful survival strategy that has independently evolved multiple times, contributing significantly to genetic diversity. Parasites have adopted various strategies to survive, including evading host immune systems and establishing symbiotic relationships with the host's microorganisms. Due to the adaptability of helminths to different environments throughout their life cycles, which enables them to modulate the hosts' immune responses, AMPs derived from parasites could offer promising leads for drug development, as they have the potential to be effective against pathogens without being overly toxic [20]. Therefore, we investigate a specific peptide, TSO8 peptide identified in *Taenia solium,* to bring more focus on the helminth AMPs and investigate their potential as a novel drug against infectious diseases.

2 Methodology

In this work, molecular dynamics simulations were performed on systems containing antimicrobial peptides, membrane model and solvent. Molecular dynamics simulations are a powerful computational technique used in various scientific disciplines, such as chemistry, biophysics, materials science, and drug discovery [17, 21-23]. Simulations can often be used to address specific questions about the properties of a model system more easily than experiments on the actual system, as they provide information of individual particle motion as a function of time. In research these methods go hand in hand, as experimental data is needed to validate the methodology. Three most common types of applications of simulation methods in the macromolecular area are [24]:

1. Determining and refining structures from data obtained by experiments, i.e., sampling the configuration space.
2. Obtaining structural and motional properties of the system at equilibrium, as well as the values of thermodynamic parameters.
3. Examining the development of the system over time.

Though the first two areas can be examined with other simulation methods, like Monte Carlo simulations, information about the development of motion in time can only be provided by MD simulations. At the core of MD simulations for biomacromolecules lies a mathematical function $U(r_1, \dots, r_N)$ which represents the total potential energy of the N particle system. This function is an approximation of a true quantum mechanical wavefunction and is dependent not only on the atomic coordinates $r_i = (x_i, y_i, z_i)$, but also on a set of parameters that describe different interparticle interactions. A combination of this potential function with properly defined parameters yields a force field. Each force field has its own set of optimized parameters that define bonded energy term U_{bonded}, nonbonded energy term $U_{nonbonded}$ and specific energy terms U_{other} [15, 24-27].

The total energy of the system is defined as:

$$U_{total} = U_{bonded} + U_{nonbonded} + U_{other} \tag{2.1}$$

$$U_{bonded} = \sum_{bonds} K_b(b - b_0)^2 + \sum_{angles} K_\theta(\theta - \theta_0)^2 + \sum_{dihedrals} K_\chi[1 + \cos(n\chi - \sigma)] \tag{2.2}$$

$$U_{nonbonded} = \sum_{nonbonded\ pairs\ ij} \left(\varepsilon_{ij} \left[\left(\frac{\sigma_{min,ij}}{r_{ij}} \right)^{12} - 2 * \left(\frac{\sigma_{min,ij}}{r_{ij}} \right)^{6} \right] + \frac{q_i q_j}{r_{ij}} \right) \tag{2.3}$$

In equation 2.2, the first sum accounts for stretching of bonds, where b, b_0 and K_b represent bond length, equilibrium bond length and stiffness constant respectively. The second term accounts for bending of valence angles, where θ, θ_0 and K_θ represent the angle formed by the

two bond vectors, equilibrium angle and stiffness constant respectively. Both terms evidently have a form of harmonic potential. The final sum accounts for dihedral or torsional rotations, which are periodic by nature so are represented by a cosine function, where χ and K_χ represent the value of dihedrals and the parameter that defines barrier heights respectively, σ is the phase and n defines periodicity. All bounded parameters are usually referred to as internal or intramolecular [15, 25, 27].

Equation 2.3 represents nonbonded energy which is composed of two parts., the first one being the Lennard-Jones equation $\left[\left(\frac{\sigma_{min,ij}}{r_{ij}}\right)^{12} - 2 * \left(\frac{\sigma_{min,ij}}{r_{ij}}\right)^{6}\right]$, which models attractive dispersion and repulsive Pauli-exclusion interactions, and the second being Coulomb's law modelling the electrostatic interaction between nonbonded pairs of atoms. ε_{ij} is a parameter describing the potential depth, r_{ij} is the distance between atoms, $\sigma_{min,ij}$ defines the distance at which the LJ energy is at its minimum, and q_i is the charge of the i-th atom. These parameters are usually referred to as interaction or external parameters. An important note is that nonbonded interactions involve only pairs of atoms [15, 25, 27].

There is a number of different force fields available, with CHARMM, GROMOS, Amber, Martini and OPLS being the most widely used force fields for simulations of protein systems. CHARMM, GROMOS, Amber and OPLS are atomistic models or all-atom (AA) models in which each atom is explicitly modelled along with its associated parameters [25]. On the other hand, Martini is a coarse-grained model, that groups multiple atoms into a single interaction site which represents a group of atoms or a molecular fragment, instead of representing each atom individually. While this simplified representation of the system comes with a compromise in accuracy and detail, it has proven to be a valuable approach in probing the spatial and temporal scales of systems that surpass the capabilities of traditional AA models [28]. Each force field contains its own set of optimized parameters and specific energy terms U_{other}, and treat different types of particles differently.

CHARMM, GROMOS and MARTINI for example include an energy term which accounts for improper dihedral torsion, or out-of-plane distortion [15, 27]:

$$U_{impropers} = \sum_{impropers} K_{imp}(\varphi - \varphi_0)^2 \qquad 2.4$$

where φ, φ_0 and K_{imp} represent improper dihedral angle, equilibrium improper dihedral angle and improper dihedral force constant, respectively.

In addition to that, CHARMM force field also includes an Urey-Bradley angle term, which describes the interaction of two terminal atoms (1,3) in an angle [15, 26]:

$$U_{U-B} = \sum_i K_{U-B}\left(r_{1,3} - r_{1,3;0}\right)^2 \qquad 2.5$$

where $r_{1,3}$, $r_{1,3;0}$ and K_{U-B} represent 1,3 atom distance, 1,3 atom equilibrium distance and the Urey-Bradley dihedral force constant, respectively.

The time evolution of the thermodynamic system, i.e., the macromolecule, composed of N particles (atoms), is given by Newtonian equation of motion:

$$m_i \frac{d^2 \boldsymbol{r}_i}{dt^2} = F_i = -\nabla_i V(\boldsymbol{r}_1, \boldsymbol{r}_2, \dots, \boldsymbol{r}_N) \qquad i = 1, \dots, N \qquad 2.6$$

with m_i, $\boldsymbol{r}_i$ being the mass and position of the i-th particle respectively, F_i being the force acting on the i-th particle and $V(\boldsymbol{r}_1, \boldsymbol{r}_2, \dots, \boldsymbol{r}_N)$ being the potential energy function, which is equivalent to equation 2.1. This set of coupled differential equations can be solved by defining initial conditions for each atom in the system: initial configuration is usually generated by 3D modelling programs such as QUARK [29] or obtained from databases like Protein Data Bank (PDB) [30] initial velocities are generated according to the defined temperature, and time steps are usually between 2 and 4 fs (1 fs= 10^{-15} s).

3 Aims and scope of the thesis

Study details around a helminth antimicrobial peptide TSO8 (see Table 4.1) identified in *T. solium*, along with its linear analogue, obtained by replacing cysteine residues with alanine residue, and 5 of its specific fragments. TSO8_lin was selected to elucidate the role of the disulfide bridge forming between the two cysteine residues. TSO8(1-23) and TSO8(20-39) were selected to examine the role of N-terminal α-helix and C-terminal coil, respectively. TSO8(3-39) and TSO8(3-23) were selected to elucidate the role of the aromatic residue (tryptophan W) at the 2nd position, which is believed to be crucial for the helical stability [31]. Molecular dynamics simulations were performed on all fragments in water and in the vicinity of a membrane model, to understand the roles of different structural motifs on the stability and activity of the peptide. TSO8(1-39) was selected to further investigate the association of peptides in water and on the membrane surface and the role of associations in its mode of action.

4 Materials and methods

4.1 Previous findings and selection of the peptide and its fragments

This study continues upon the results presented in the master's thesis by Roko Čopac [18]. In said thesis, TSO8 was selected for analysis based on the specificity in predicted structuring, favourable biophysical properties and considering its uniqueness from the biological diversity point, in investigation detailly explained in thesis.

The study utilized protein translations from annotated gene models in the *T. solium* genome version Tsolium_Mexico_v1. An in-house script was employed to identify potential AMPs by screening for proteins with characteristics typical of AMP precursors, such as a length less than 200 amino acids and a supported signal peptide for secretion. In the resulting peptides, the presence of a specific amphipathic α-helix signature associated with antibacterial peptides was confirmed. Initial identification yielded three candidate peptides, which were further analysed using BLASTp and tBLASTn searches to identify related peptides. Additional searches were conducted against the *T. solium* genome and transcriptome, and homologous peptides were sought in other Cestoda species' genomes. The identified peptides were then subjected to sequence alignment to ensure their validity, with only full-length proteins considered for further analysis. Amongst these candidates was the focus of this work, TSO8 peptide, for which the BLASTp search against non-redundant database resulted in only six peptides with significant similarity (E-value <0.05) with other sequences, while tBLASTn search against whole genome shotgun contigs (wgs) database resulted in no similar peptides [18].

TSO8 peptide consists of 39 amino acids and has a relatively high net charge of +15.9 at pH 7.0. Linear TSO8 sequence was obtained by replacing alanine residues, leading to the removal of the disulfide bonds, and has a net charge of +16.0 at pH 7.0.The peptide charges were calculated by BACHEM peptide calculator. Several TSO8 fragments were synthesized to explore the role of glycine followed by tryptophan (GW) at the N-terminal, as well as roles of both N-terminal and C-terminal domains [18].

Table 4.1 TSO8 fragment sequences with defined N- and C-terminals.

Peptide	Sequence	Length
TSO8 (1-39)	NH_3^+-GWRRLRRSIRRRIRRIFRKPRRICFPYCPKGPKKGRGDF-COO^-	39 AA
TSO8_lin	NH_3^+-GWRRLRRSIRRRIRRIFRKPRRIAFPYAPKGPKKGRGDF-COO^-	39 AA
TSO8 (3-39)	NH_3^+-RRLRRSIRRRIRRIFRKPRRICFPYCPKGPKKGRGDF-COO^-	37 AA
TSO8 (1-23)	NH_3^+-GWRRLRRSIRRRIRRIFRKPRRI-$CONH_2$	22 AA
TSO8 (3-23)	NH_3^+-RRLRRSIRRRIRRIFRKPRRI-$CONH_2$	20 AA
TSO8 (20-39)	CH_3CONH-PRRICFPYCPKGPKKGRGDF-COO^-	20 AA

The study included circular dichroism spectroscopy, determination of antimicrobial activity towards Gram-negative and Gram-positive strains, toxicity towards human cell lines and molecular modelling.

Structural analysis using circular dichroism spectroscopy in solutions of different TFE concentrations (0%-50%) as well as in SDS shows that all candidates are unstructured in aqueous environment but start forming helical structures as the TFE concentration increases, in slightly different manor. TSO8(1-39) has the lowest percentage of helical content, 7.2% and 9.2% in solutions with 50% TFE and SDS, respectively. TSO8(3-39) has a slightly higher helicity, with 13.3% and 16.2% of helical content in 50% TFE and SDS respectively. On the other hand, N-terminal fragments TSO8(1-23) and TSO8(3-23), have a much higher helicity, with the former having slightly higher percentage of helical content (32.5% in 50% TFE and 20.9% in SDS) than the latter (28.7% in 50% TFE and 16.2% in SDS), which elucidates the contribution of GW sequence to the increase in helicity [18].

Antimicrobial activity of the peptides was assessed by determining MIC and MBC values against both Gram-positive (*S. aureus*) and Gram-negative (*E. coli*) bacterial strains. Amongst the TSO8 fragments, the most potent was TSO8(3-39) and the least potent was TSO8(3-23). Results suggest that GW sequence might have an effect on potency of shorter fragments, which can be connected to its contribution to the increase of helical content, since it was explored that helicity has a high effect on potency [18].

Table 4.2 Antimicrobial activity of TSO8 fragments (results obtained from [18]).

	E. coli		*S. aureus*	
Fragment	MIC [μM]	MBC [μM]	MIC [μM]	MBC [μM]
TSO8(1-39)	2	2	8	8
TSO8(3-39)	1	1	4	4
TSO8_lin	-	-	-	-
TSO8(1-23)	4	4	2	2
TSO8(3-23)	8	8	4	4
TSO8(20-39)	-	-	-	-

To assess cytotoxicity of the peptides, MEC1 cells were exposed to increasing peptide concentrations. TSO8(1-39) was shown to be extremely toxic at higher concentrations. The C-terminal TSO8(20-39) fragment showed negligible toxicity even at the highest tested concentration. The rest of the fragments showed toxicity similar to the TSO8(1-39), with the TSO8(3-39) being the least toxic amongst them, again possibly showing the effect of the GW sequence on peptide activity [18].

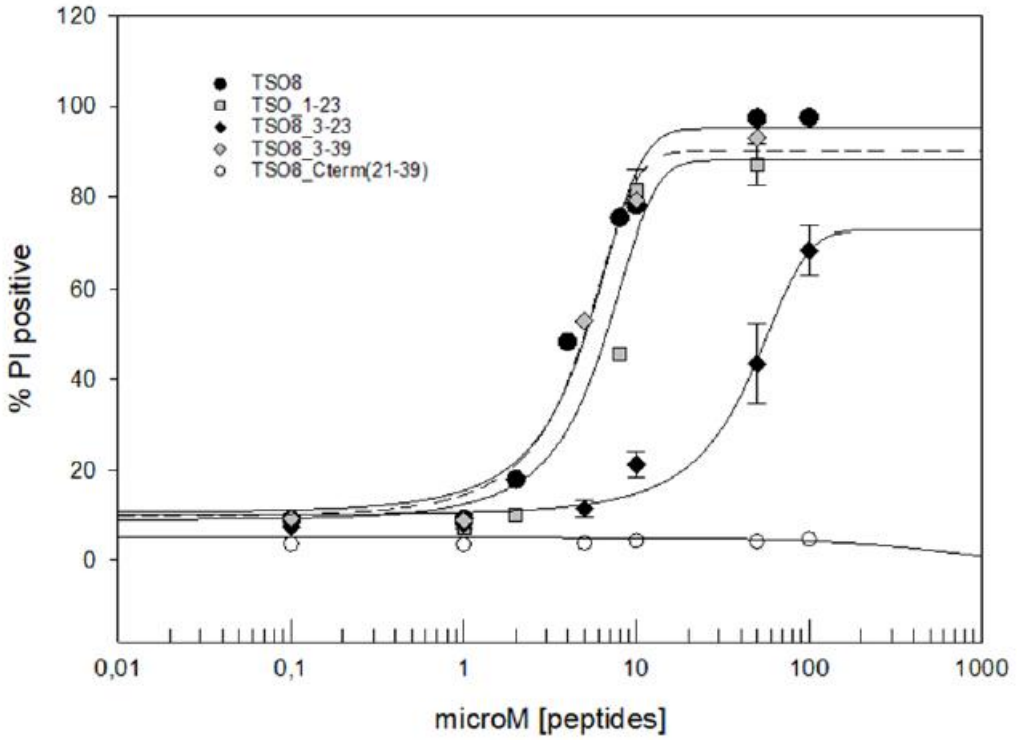

Figure 4 Cytotoxicity assay results for different concentrations of TSO8 fragments against MEC-1 cells (figure obtained from Čopac [18]).

To build upon these results and further analyse the fragments as well as propose potential models with respect to experimental data, in this thesis, molecular dynamics simulations were performed on all of them in water and in the vicinity of a membrane model.

4.2 Initial peptide structures

3D models of the initial peptide structures were obtained from Contact-assisted QUARK (cQUARK) structure predictor which is a method for *ab initio* protein structure prediction based on fragment assembly simulations [29, 32]. cQUARK predictor generates 5 models, and for TSO8(1-23), TSO8(3-23) and TSO8_lin model 1 was used as the initial structure, as it is the model with the highest TM score.

It was important to verify that the predicted models for TSO8(1-39), TSO8(3-39) and TSO8(20-39) include the formation of a disulfide bridge between two cysteine residues. In the case of TSO8(1-39) and TSO8(20-39), cQUARK successfully generated one out of five 3D models with sulphur atoms at a distance of about 2.05 Å which is the requirement for the disulfide bridge formation [33]. However, none of the 3D models predicted for TSO8(3-39) contained the disulfide bridge, which was then incorporated into one using Disulfide by Design v 2.13 (see Figure 41 in the Appendix) [34, 35].

The Eisenberg 2D hydrophobic moments were calculated using *HeliQuest* online calculator [36] to examine the amphipathicity of TSO8(1-39) and TSO8(3-39). The 2D hydrophobic moment measures amphipathic structure for an ideal α-helix, therefore the results are presented

only for the α-helical sequence of TSO8(1-39) in Figure 5 and TSO8(3-39) in Figure 6, which includes residues from 1 through 19 (or 3 through 19). The results indicate an amphipathic structure for both peptides, with TSO8(1-39) having a slightly higher 2DHM value. The α-helical segment of TSO8(1-39) has a distinct hydrophobic face, which is absent in TSO8(3-39) due to the lack of tryptophan (W) residue.

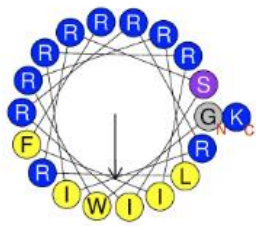

Hydrophobicity (H)	Polar residues + Gly (n/%)	Nonpolar residues (n/%)
0.001	13/68.42	6/31.58
Hydrophobic moment (μH)	Uncharged residues + Gly	Aromatic residues
0.696	Ser 1, Gly 1	Trp 1, Phe 1
Net charge (z)	Charged residues	Special residues
11	Lys 1, Arg 10	-
Hydrophobic face: L I I W I		

Figure 5 Properties of TSO8(1-39) α-helical sequence (first 19 residues). Hydrophobic residues are coloured yellow, polar charged (+) blue, polar uncharged violet, and glycine grey.

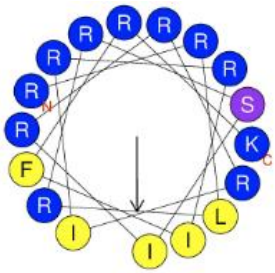

Hydrophobicity (H)	Polar residues + Gly (n/%)	Nonpolar residues (n/%)
-0.132	12/70.59	5/29-41
Hydrophobic moment (μH)	Uncharged residues + Gly	Aromatic residues
0.648	Ser 1	Phe 1
Net charge (z)	Charged residues	Special residues
11	Lys 1, Arg 10	-
Hydrophobic face: none		

Figure 6 Properties of TSO8(3-39) α-helical sequence (first 17 residues). Hydrophobic residues are coloured yellow, polar charged (+) blue and polar uncharged violet.

4.3 Simulation setup

All-atom MD simulations were performed using the Gromacs (Groningen machine for chemical simulations) 2021.3 package [37] on the supercomputer Bura at University of Rijeka [38].

4.3.1 Initial conformations

CHARMM-GUI *Solution Builder* [39, 40] was used to generate initial conformations of single peptides solvated in water, and CHARMM-GUI *Membrane Builder* [41, 42] was used to generate initial conformations of solvated peptides in the vicinity of a membrane model. For all simulations a CHARMM36m [43] force field was used, and the TIP3 [44] water molecule model. The simulation boxes for a single solvated protein system were cubic, with sizes fit to the protein size, maintaining a 2 nm edge distance, and two simulation cases starting from different velocities were performed.

Simulation on multiple TSO8(1-39) peptides were also performed in water, to examine possible aggregations, for which the initial structures were generated using CHARMM-GUI *Multicomponent Assembler* [39, 45]. Simulation box was cubic with the side length of 6.026 nm.

To investigate peptide-membrane interaction, the inner bacterial membrane model was used, whose main lipid components are phosphatidylethanolamine (PE) and phosphatidylglycerol (PG). The model membrane was built as a negatively charged bilayer consisting of palmitoyl oleoyl PE (POPE) and palmitoyl oleoyl PG (POPG) in the proportion 3:1 [46], specifically 96 POPE and 32 POPG molecules per layer. Lipid models were obtained from CHARMM-GUI *Individual Lipid Molecule Library* [47]. Single solvated peptides were placed on an x-y plane perpendicular to the membrane surface, about 2 nm above the membrane. A layer of water molecules, with a minimum 4 nm thickness, was added above and below the peptide-membrane system, which resulted in approximately 100 molecules of water per lipid.

Furthermore, simulations on multiple TSO8(1-39) peptides with the membrane were performed in order to investigate their association on the membrane surface and potential pore formation. Similarly to the systems containing single peptides near the membrane, 6 and 12 TSO8(1-39) peptides were placed about 2 nm above the membrane surface, perpendicular to each other. This time, the model membrane consisted of a total of 592 lipids (222 POPE and 74 POPG per layer) and the layer of water molecules was added with a minimum 5 nm thickness which resulted with around 120 water molecules per lipid. Also, simulations with a larger number of peptides having longer sequences can be challenging as described in section 8.2 in the Appendix.

All systems were neutralized by adding K^+ and CL^- ions at a 0.15 M concentration using the distance ion placing method [44].

4.3.2 Energy minimization and equilibration

Energy minimization of all systems was performed using the steepest descent algorithm. Solvated peptide systems were equilibrated for 125 ps in the isothermal isochoric (NVT) ensemble at a temperature of 310 K (or 380 K for the system with 6 peptides), with harmonic restraints on peptide backbone $\left(k = 1\frac{kcal}{molÅ}\right)$ and side chains $\left(k = 0.1\frac{kcal}{molÅ}\right)$. Peptide-membrane systems were equilibrated as per CHARMM-GUI *Membrane Builder* [41, 42] recommendation in six steps, with decreasing harmonic restraints (see Table 8.5 in Appendix The first two steps of the equilibration were carried out in the isothermal isochoric (NVT) ensemble, and the rest were carried out in the isothermal isobaric (NpT) ensemble. Berendsen thermostat and barostat were used in all steps, and the temperature was fixed at 310 K (or 380 K).

4.3.3 Production

In all simulations, NpT ensemble conditions were imposed by the Nose-Hoover thermostat and Parrinello-Rahman barostat, with the constants of 1.0 ps for temperature and 5.0 ps for pressure, and the compressibility of $4.5 \cdot 10^{-5}$ bar [48, 49]. The Leap-frog integrator was used with a fixed timestep of 2 fs, and the bonds were handled by the LINCS algorithm [50]. Particle-Mesh-Ewald (PME) method [51] was used to calculate electrostatic interactions with the Coulomb cutoff at 1.2 nm. Van der Waals cutoff was set at 1.2 nm, with force-switch at 1.0 nm.

Simulation durations were 500 ns, 700 ns, 1 μs and 1.5 μs, depending on the system.

4.4 Analysis

3D hydrophobic moments were calculated for initial and final states of peptides in the simulations with the membrane, using the 3DHM online calculator [52], which generates the 3DHM vector from the distribution of hydrophobic and hydrophilic sections and from the charges of each atom [15].

Post-simulation analysis was performed using Gromacs tools: *rms, gyrate, helix, mindist, density*, *trajectory and clustsize* [37]. The *rms* tool calculates the root mean square deviation, while *gyrate* calculates the radius of gyration and *helix* calculates several properties, one of which is the helicity percentage over time. The *mindist* tool calculates the number of contacts and the minimum distance between a reference group of atoms and a number of other selected groups. It was used to calculate the number of contacts of hydrophobic and polar residues with P atoms in membrane lipids, with the distance value under 0.6 nm. The *density* tool was used to extract density profiles of P atoms, all peptide atoms, atoms of hydrophobic residues, atoms of polar residues, atoms of α-helix and atoms of the coil structure. The *clustsize* tool calculates the number of clusters that peptides form and the number of peptides in said clusters.

DSSP program [53] was used to generate the secondary structure over simulation time.

Charts were created using Gnuplot 5.4 [54] and Xmgrace [55] programs, and visualisation of the systems was done by VMD program [56].

5 Results

5.1 Single peptide in water

Structural stability and roles played by different specific segments of the TSO8 peptide were investigated through two cases of 500 ns long simulations of a peptide in water solution.

Presentation of the results is according to two groups. The first group comprises of the full mature TSO8(1-39) peptide, its linear analogue TSO8_lin, and the full peptide without the initial GW sequence TSO8(3-39) chosen to assess the influence of the GW sequence and disulfide bond, while the second group consists of the shorter helical fragment TSO8(1-23), helical fragment lacking the initial GW sequence TSO8(3-23) and the coil-like fragment TOS8(20-39), to compare the behaviour of the N-terminal α-helix and C-terminal coil regions.

5.1.1 Long peptides in water

Figure 7 illustrates the initial conformations and those observed at the 500 ns simulation time for two simulation cases. TSO8(1-39) displays stability of its N-terminal α-helix during the simulation time in case 1, where the conformational changes are only present in the unstructured C-terminal segment. However, in case 2, it exhibits some more structural changes, showcasing a loss of its initial helical content to some extent. On the other hand, the full peptide without the initial GW sequence, TSO8(3-39), demonstrates a lack of stability and loses more of its initial helical structure at the N-terminal. The linear analogue TSO8_lin preserves less structuring of the N-terminal helix compared to TSO8(1-39), but slightly more compared to TSO8(3-39) during the simulation time of 500 ns. Furthermore, it exhibits more structural changes in the C-terminal region then both TSO8(1-39) and TSO8(3-39).

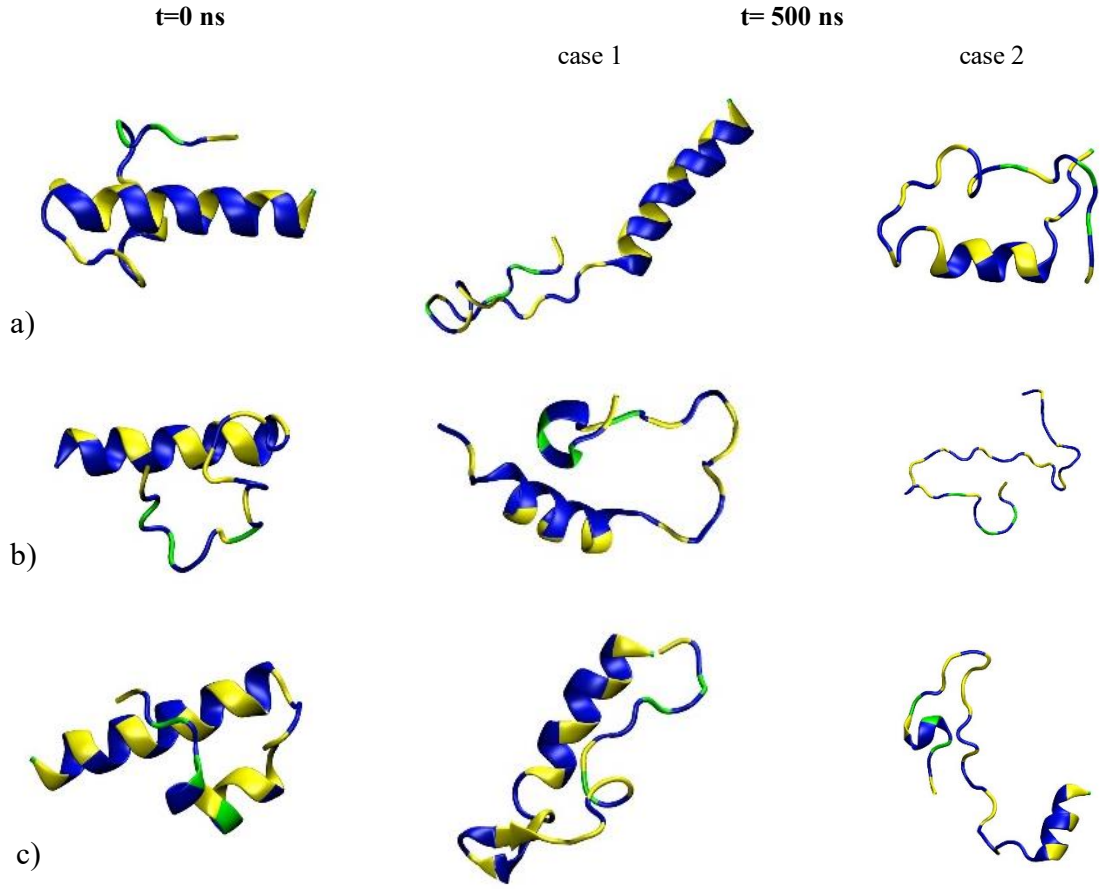

Figure 7 Snapshots from simulations of single peptide in water, where the initial conformation is shown on the left and those at the 500 ns simulation time in the middle (case 1) and on the right (case 2) for: a) TSO8(1-39), b) TSO8(3-39) and c) TSO8_lin. Amino acids are coloured according to their hydrophobicity (polar – blue, hydrophobic – yellow, glycine - green). Water molecules and ions are not shown for clarity.

DSSP secondary structure analysis confirms the persistence of the N-terminal α-helix of TSO8(1-39) throughout the 500 ns simulation time in case 1, as presented in Figure 8 a. In case 2, the peptide exhibits loss of its initial helical structure for the first 7 residues, while still preserving the rest of it.

Figure 8 b depicts results for TSO8(3-39), which indicate a loss of its N-terminal helical structure for the first 5 residues from around 30 ns in both cases. In case 1, TSO8(3-39) also shows loss of the helical structure for the 13th to 16th residues at around 380 ns of the simulation time. In case 2, this fragment exhibits more structural changes, leading to the complete loss of its initial helical structure for the last 10 ns. These disruptions correlate with an increase in RMSD and radius of gyration, as illustrated in Figure 42 and Figure 43 in the Appendix.

The initial N-terminal helical structure is also preserved for TSO8_lin in case 1, as seen from Figure 8 c. In case 2, TSO8_lin exhibits more structural changes, especially after 300 ns simulation time, where it showcases a trend of α-helix unfolding for the C-terminal end but preserving its initial helicity only for the first 10 residues. However, DSSP predicts the

formation of β-sheets in both cases, which are more prominent in case 1. This accounts for the lower values of RMSD and radius of gyration observed compared to TSO8(1-39) (see Figure 42 and Figure 43 in the Appendix). These results suggest that peptides lacking disulfide bonds exhibit greater flexibility to adopt alternative structural motifs such as β-sheets, implying that the role of disulfide bonds may be in preserving the C-terminal unstructured configuration.

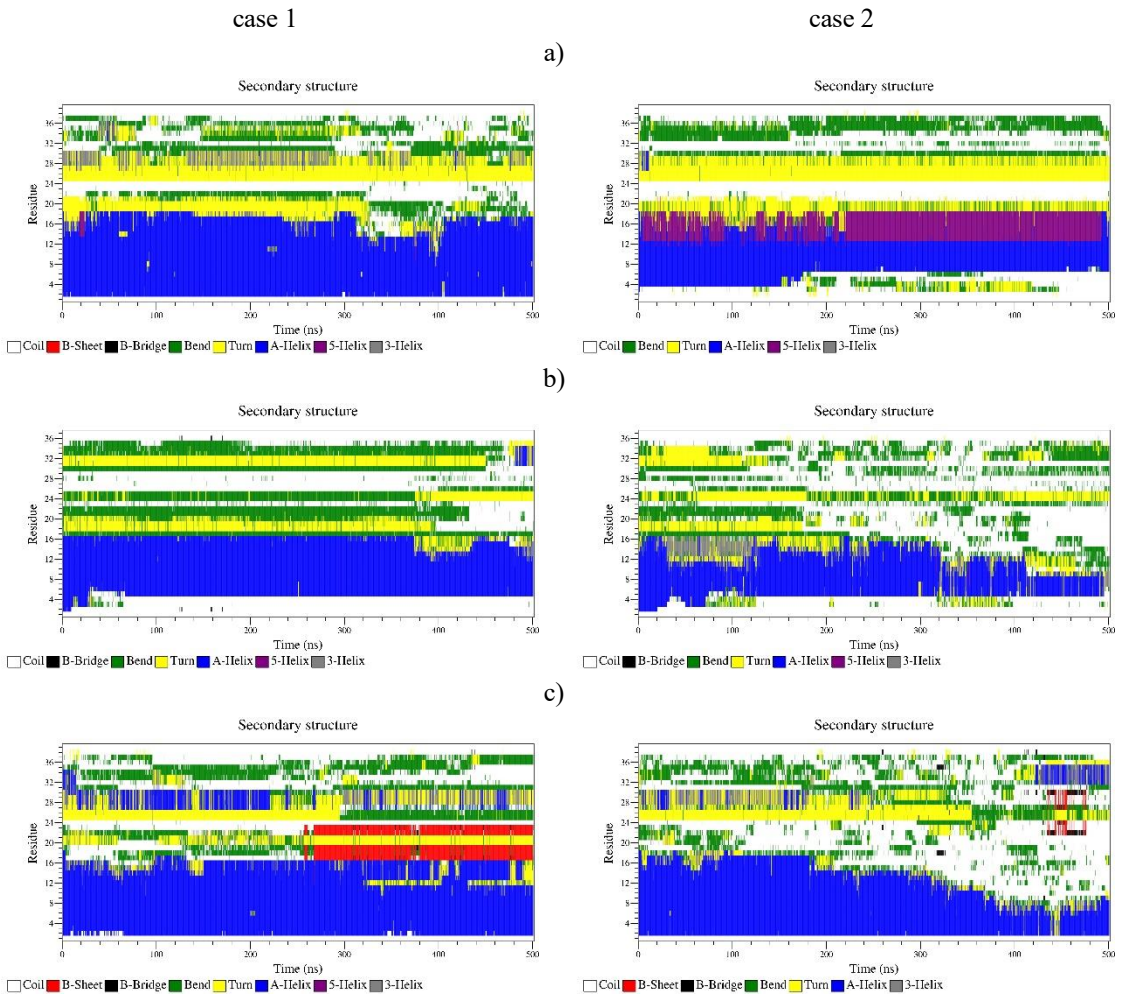

Figure 8 DSSP analysis for 500 ns long simulations of single peptides in water, where case 1 is on the left and case 2 on the right for: a) TSO8(1-39), b) TSO8(3-39) and c) TSO8_lin.

The trend of peptide behaviour is similar in both cases: TSO8(1-39) once again proves to be the most stable, while TSO8(3-39) loses more of its initial helical content than both TSO8(1-39) and TSO8_lin.

5.1.2 Short peptides in water

Shorter TSO8 fragments were analysed to further understand the functions of the N-terminal GW sequence. Figure 9 illustrates the initial conformations and the ones at 500 ns long simulation. TSO8(1-23) exhibits less stability compared to the full TSO8(1-39) peptide while still preserving its initial helical structure to some extent. On the other hand, the short fragment lacking the initial GW sequence, TSO8(3-23) is shown to be extremely unstable, completely

losing its initial helical structure. Additionally, results are presented for the coil-like fragment TSO8(20-39), which as expected, does not show any structuring in water.

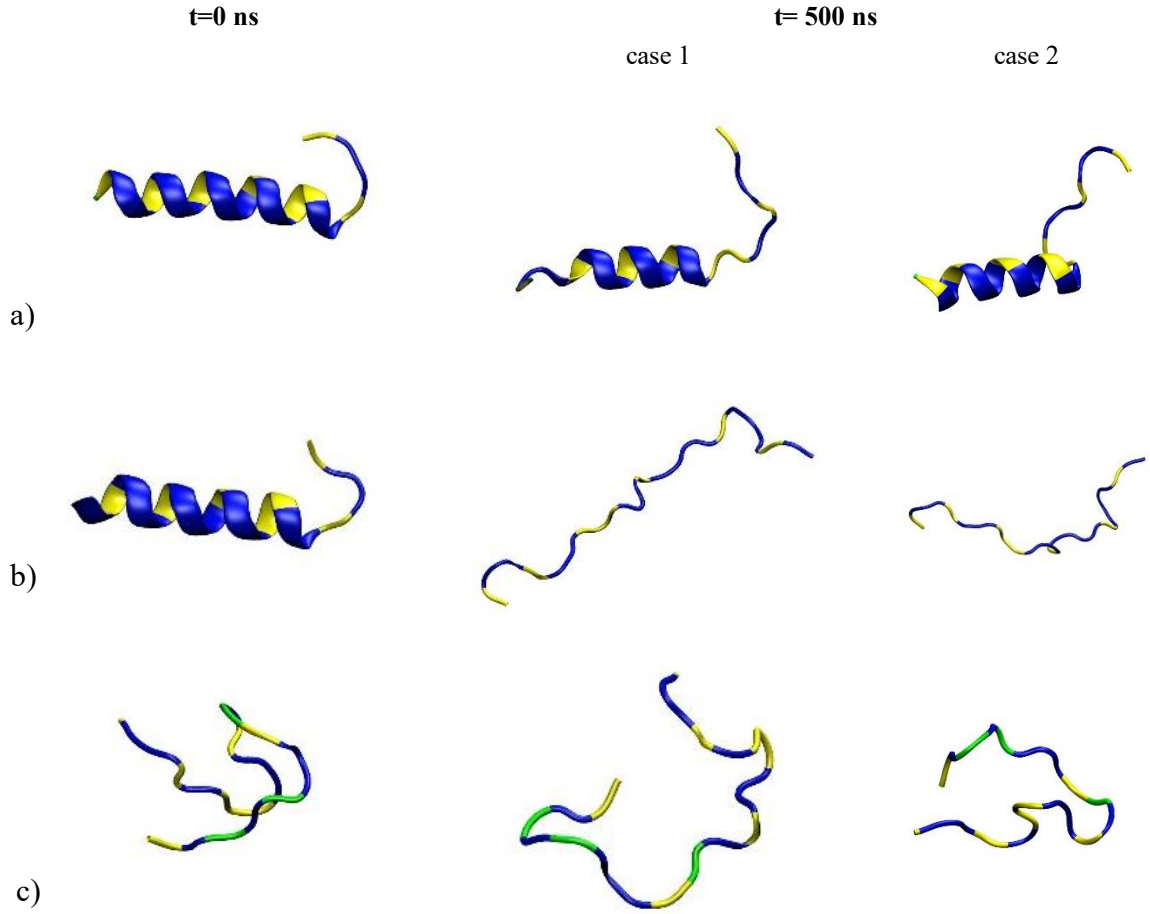

Figure 9 Snapshots from simulations of single peptide in water, where the initial conformation is shown on the left and those at the 500 ns simulation time in the middle (case 1) and on the right (case 2) for: a) TSO8(1-23), b) TSO8(3-23) and c) TSO8(20-39). Amino acids are coloured according to their hydrophobicity (polar – blue, hydrophobic – yellow, glycine - green). Water molecules and ions are not shown for clarity.

DSSP secondary structure analysis confirms that TSO8(1-23) preserves most of its helical structure in case 1, up to 300 ns, when it loses some of its helical content from both ends, as depicted in Figure 10 a. In case 2, the fragment exhibits more structural changes from its C-terminal end, but the N-terminal remains stable for the entire 500 ns simulation time. On the contrary, from Figure 10 b it can be seen that TSO8(3-23) exhibits the complete loss of its initial helical structure after less than 200 ns for both performed simulations. The time evolution for the unstructured TSO8(20-39) in water is presented as well in Figure 10 c.

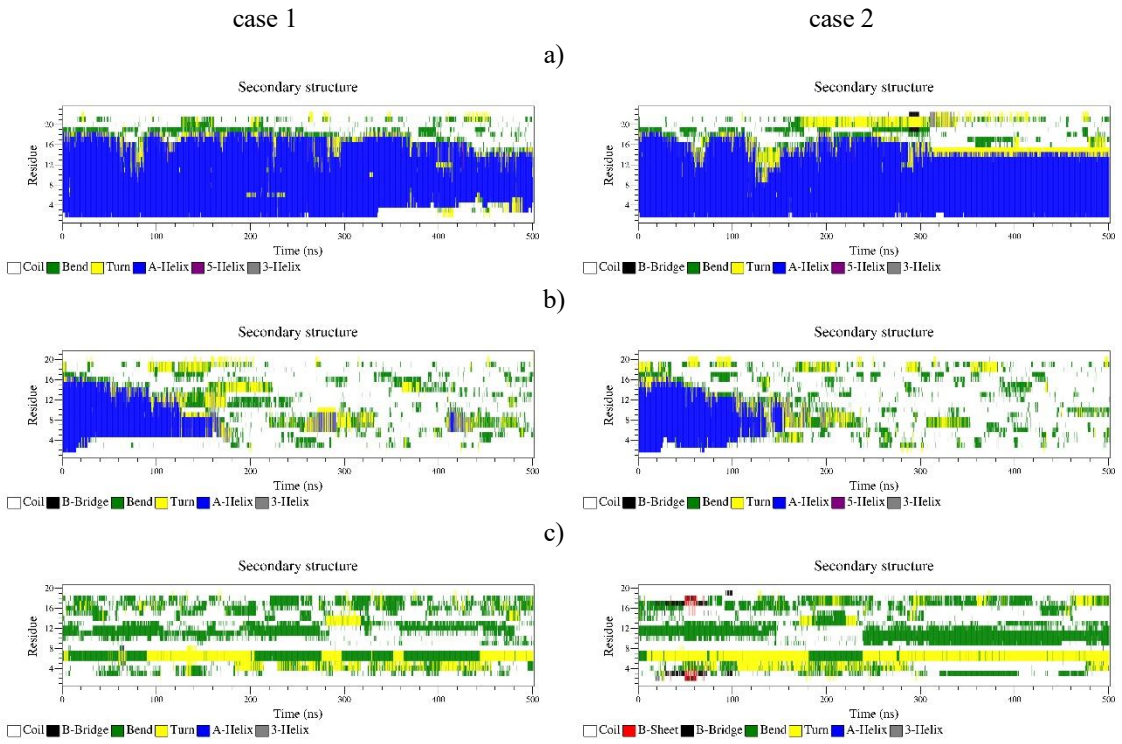

Figure 10 DSSP analysis for 500 ns long simulations of single peptides in water, where case 1 is on the left and case 2 on the right for: for: a) TSO8(1-23), b) TSO8(3-23) and c) TSO8(20-39).

5.1.3 Summary of the results for single peptides in water

Initial experiments included simulations of single peptides in water. The simulations were performed twice for each peptide, starting from different initial conditions. Results show that the full mature peptide TSO8(1-39) is quite stable in water, with its helicity mostly preserved during the 500 ns simulation time. TSO8_lin shows to have the N-terminal sequence less preserved, and possible formations of β-sheet structures, which potentially shows that the lack of the disulfide bridge gives more freedom for different structural conformations. The results of both the longer TSO8(3-39) and shorter TSO8(3-23) fragments lacking the GW sequence at the N-terminal confirm the importance of said sequence in preserving the α-helical structure. This is in line with results presented by Sato et. al [31], and experimental data presented in the master thesis by Čopac [18].

5.2 Single peptide in the vicinity of the membrane

To examine how TSO8 antimicrobial peptide interacts with the bacterial membrane, and potential contributions of the GW sequence, disulfide bridge, N-terminal α-helix and C-terminal coil to this interaction, simulations were performed placing one single peptide in the vicinity of the Gram-negative bacterial membrane model. The results are presented following the same scheme as for peptides in water, and P/L ratio was equal to 1/256 in each case.

5.2.1 Long peptides near the membrane

Interactions of TSO8(1-39), TSO8_lin and TSO8(3-39) with the membrane were observed during 1.5 μs long simulations. Peptides were initially placed about 2 nm above the membrane, as depicted in

Figure 11, and orientated so that the polar and hydrophobic residues were equally distanced from the membrane. Additionally, TSO8(1-39) was oriented in a way that its unstructured C-terminal was closer to the membrane then the N-terminal α-helix, which was not the case for other peptides. However, all peptides showcased the same behaviour in the beginning of the simulation: the rotation of the N-terminal α-helix, and the contact of its polar residues with the membrane. The first contact is due to the electrostatic interactions of the positively charged residues of the α-helix and the negatively charged membrane. However, during the 1.5 μs long simulation, peptides did not exhibit restructuring or deeper entering of the hydrophobic residues in the membrane. In each case, peptide remained in the polar membrane region during the simulation time.

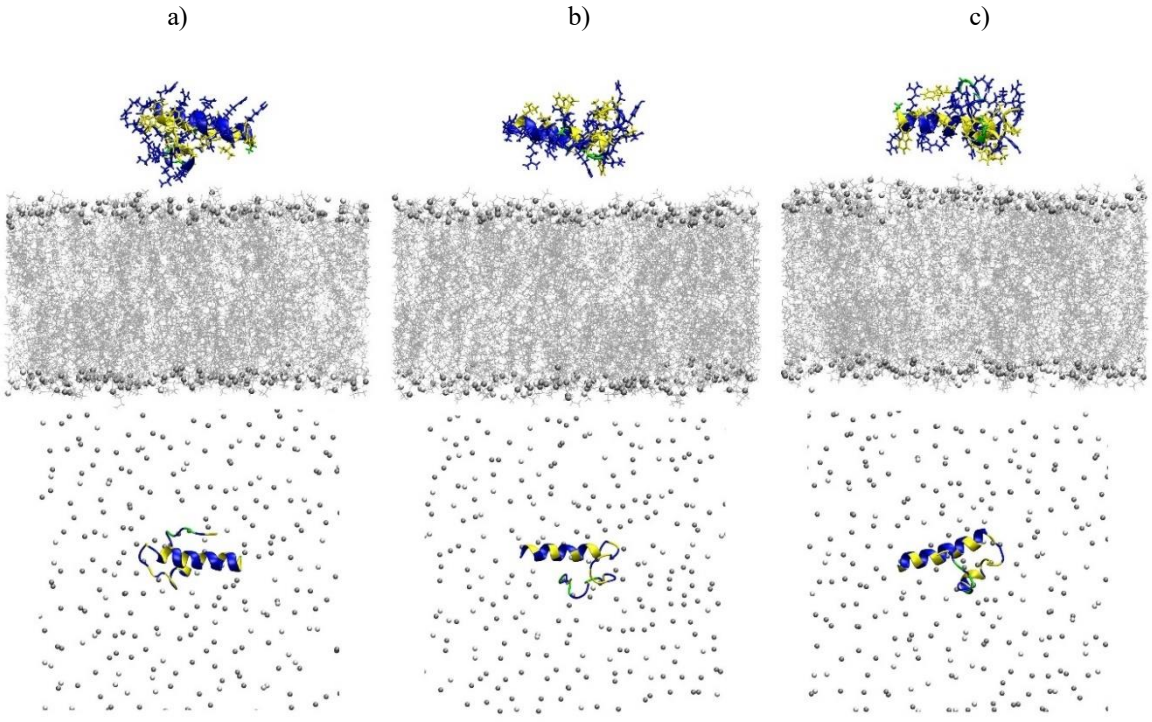

Figure 11 Initial states of peptides near the POPE:POPG membrane model as seen from the side (top) and top (bottom) for: a) TSO8(1-39), b) TSO8(3-39) and c) TSO8_lin. Amino acids are coloured according to their hydrophobicity (polar – blue, hydrophobic – yellow, glycine - green). Membrane is coloured by residue name (POPE – silver, POPG - white). Water molecules and ions are not shown for clarity.

Figure 12 illustrates the interaction of TSO8(1-39) with the membrane during the simulation time and shows how its N-terminal α-helix is preserved and stays in contact with the membrane, while the unstructured C-terminal remains on the outside of the membrane throughout the simulation.

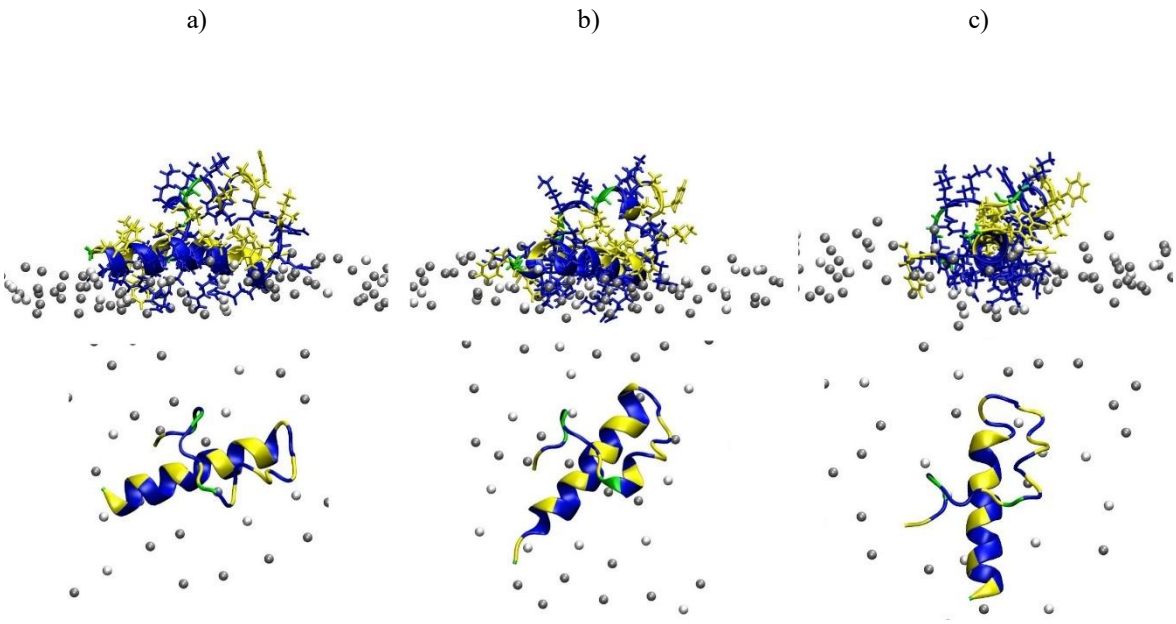

Figure 12 Snapshots from 1.5 μs long simulation of TSO8(1-39) near the POPE:POPG membrane. Side (top) and top (bottom) view of peptide states at times a) t=100 ns, b) t= 500 ns and c) t =1.5 μs. Amino acids are coloured according to their hydrophobicity (polar – blue, hydrophobic – yellow, glycine - green). Membrane is represented only by P atoms of the upper leaflet (POPE – silver, POPG - white). Water molecules and ions are not shown for clarity.

Figure 13 illustrates the behaviour of TSO8(3-39) during the 1.5 μs long simulation with the membrane. Similar to TSO8(1-39), it also has its N-terminal α-helix preserved and in contact with the membrane, but the C-terminal coil does not seem to be surrounding it on the outside and is slightly contacting the membrane, which can be confirmed from the density profiles of C-terminal coil shown in Figure 19 and a higher number of contacts compared to the other fragments shown in Figure 18.

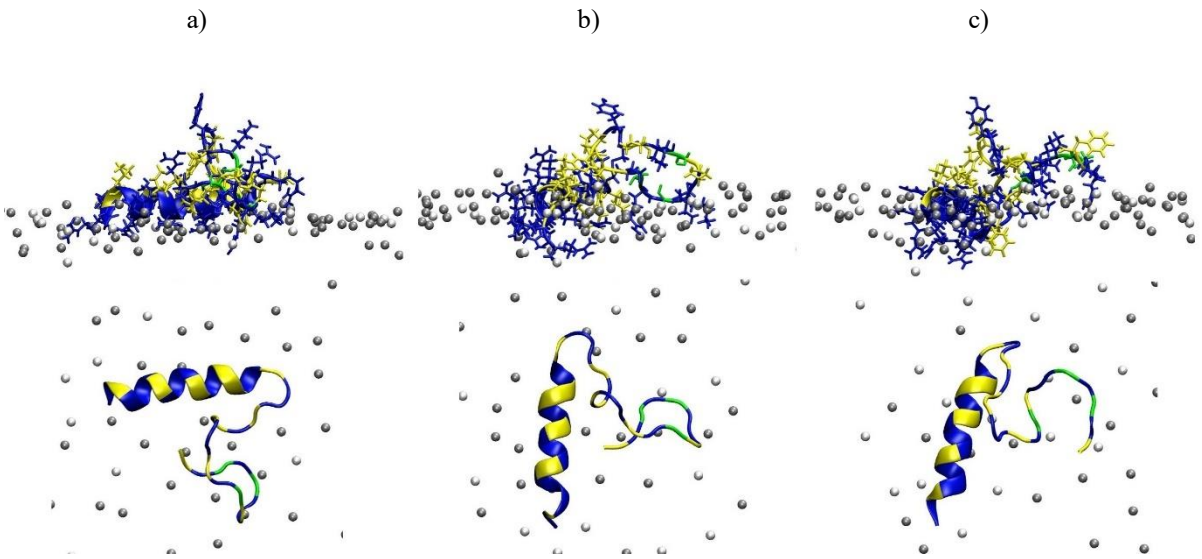

Figure 13 Snapshots from 1.5 μs long simulation of TSO8(3-39) near the POPE:POPG membrane. Side (top) and top (bottom) view of peptide states at times a) t=100 ns, b) t= 500 ns and c) t =1.5 μs. Amino acids are coloured according to their hydrophobicity (polar – blue, hydrophobic – yellow, glycine - green). Membrane is represented only by P atoms of the upper leaflet (POPE – silver, POPG - white). Water molecules and ions are not shown for clarity.

Finally, the behaviour of TSO8_lin during the 1.5 μs simulation, depicted in Figure 14, is similar to the one observed in the case of TSO8(1-39).

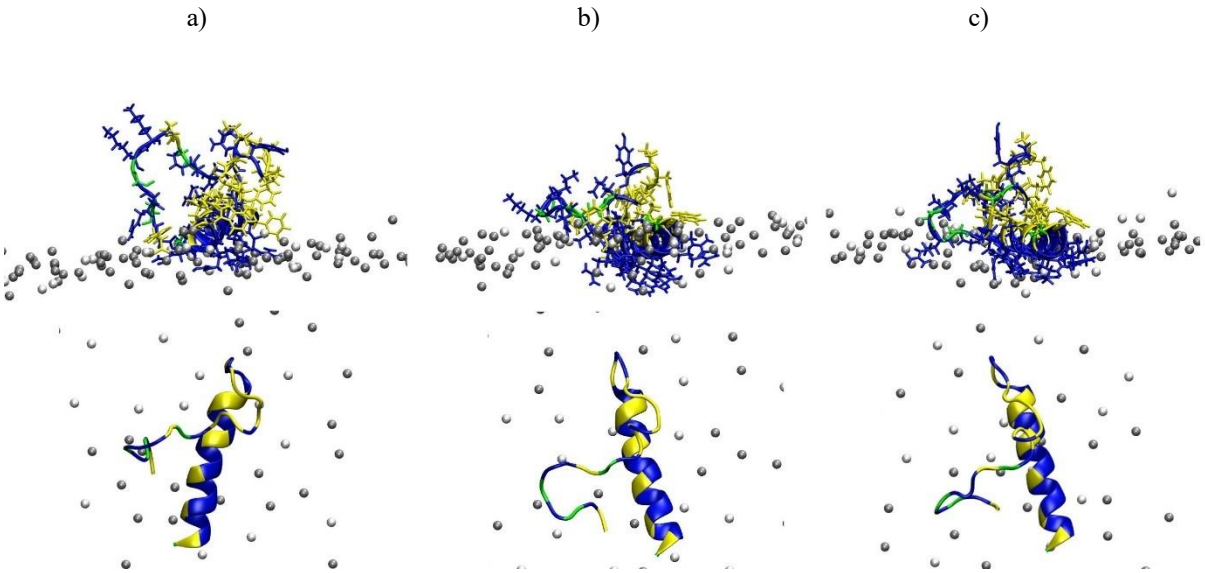

Figure 14 Snapshots from 1.5 μs long simulation of TSO8_lin near the POPE:POPG membrane. Side (top) and top (bottom) view of peptide states at times a) t=100 ns, b) t= 500 ns and c) t =1.5 μs. Amino acids are coloured according to their hydrophobicity (polar – blue, hydrophobic – yellow, glycine - green). Membrane is represented only by P atoms of the upper leaflet (POPE – silver, POPG - white). Water molecules and ions are not shown for clarity.

The 3DHMs were calculated in each case for the initial and final (1.5 μs) configurations, as measures of the amphipathicity of the peptides. The results presented in Table 5.1, Figure 15 and Figure 16, show that 3DHM increases and orients in such way that the vector points away from the membrane surface. This vector orientation is not favourable for peptide insertion, as indicated also by the electrostatic potential maps of the peptide surfaces, where blue colour indicates the positively charged regions. At both the initial and final moment of the simulation, values of 3DHM and the angle between the 3DHM vector and z axes, are lowest for the full peptide TSO8(1-39) and highest for TSO8(3-39). This was expected from the visualisation of the states, since the C-terminal coil of TSO8(3-39) is closer to the membrane leaving the upper residues of the α-helix open for possible reorientation.

Table 5.1 Absolute values of 3DHM calculated for the initial and final (t=1.5 μs) configurations of TSO8(1-39), TSO8(3-39) and TSO8_lin for simulations near the membrane. The results were obtained using two different dielectric constants: for the initial position of the peptide in water, dielectric constant was 78.5, while for the final position of the peptide at the interface of membrane and water the dielectric constant was 20.0 [15].

Peptide	3DHM at t=0ns [ÅkT/e]	3DHM at t=1.5μs [ÅkT/e]
TSO8(1-39)	5.350	32.681
TSO8(3-39)	17.589	84.074
TSO8_lin	10.111	48.814

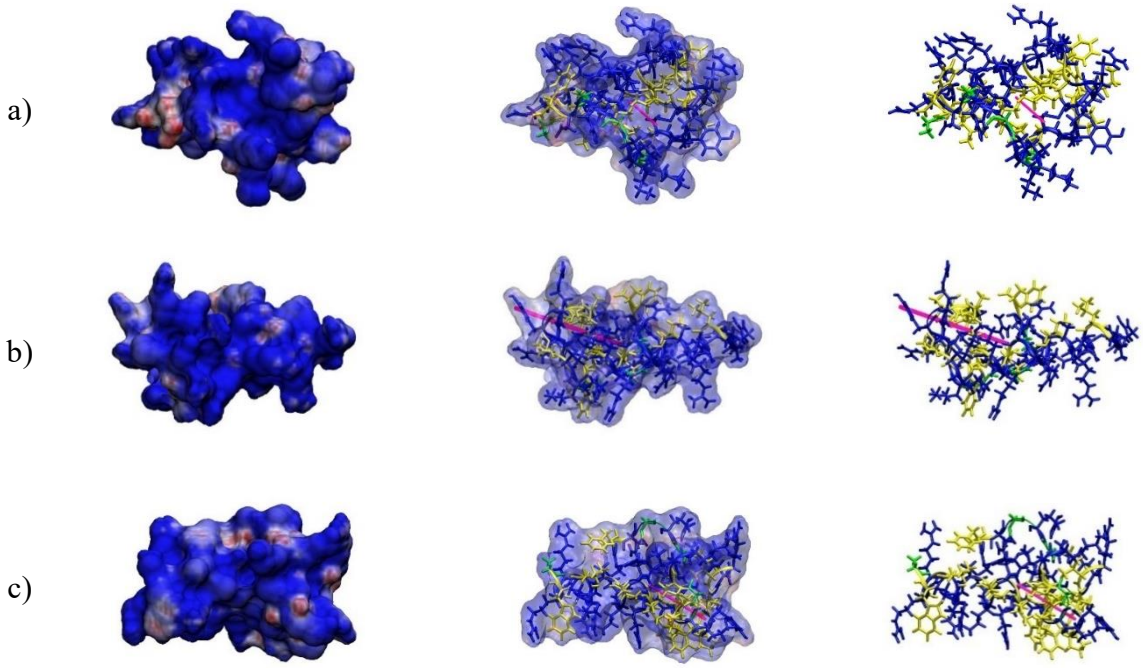

Figure 15 3DHM calculations where the electrostatic potential map of the peptide surface is shown on the left (opaque) and in the middle (transparent), and peptide structure with the 3DHM vector is shown on the right for: a) TSO8(1-39), b) TSO8(3-39) and c) TSO8_lin at the initial time of the simulations with POPE:POPG membrane (not shown for clarity). Peptides are parallel to the membrane surface. Hydrophobic residues are coloured yellow, polar residues blue and glycine residues green. 3DHM vector is coloured magenta. Positively charged regions of the electrostatic potential are coloured blue, and negatively charged regions are coloured red.

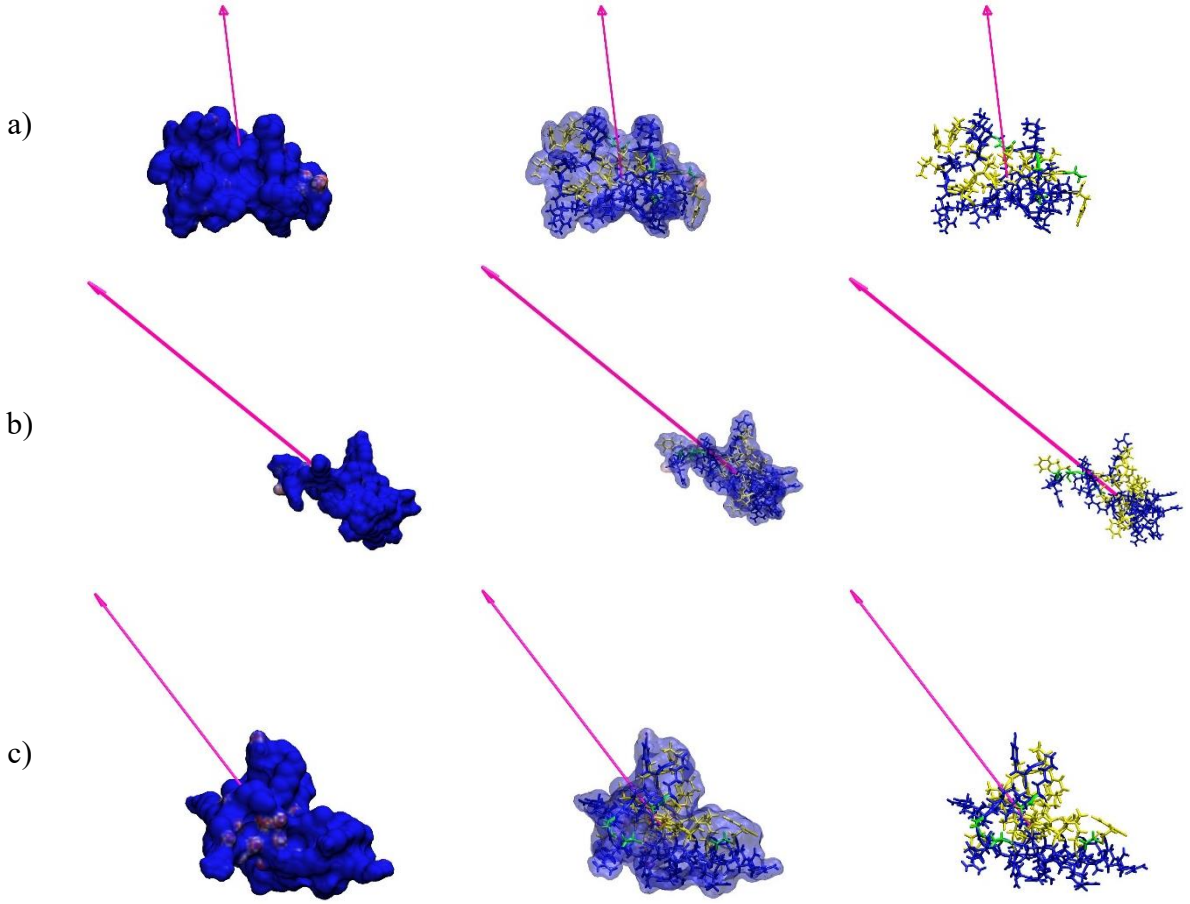

Figure 16 3DHM calculations where electrostatic potential map of the peptide surface is shown on the left (opaque) and in the middle (transparent), and peptide structure with the 3DHM vector is shown on the right for: a) TSO8(1-39), b) TSO8(3-39) and c) TSO8_lin at the final (1.5 μs) time of the simulations with POPE:POPG membrane (not shown for clarity). Peptides are parallel to the membrane surface. Hydrophobic residues are coloured yellow, polar residues blue and glycine residues green. 3DHM vector is coloured magenta. Positively charged regions of the electrostatic potential are coloured blue, and negatively charged regions are coloured red.

To further examine the behaviour of hydrophobic and polar residues during the simulations, density profiles were calculated as average for the first and last 100 ns of the simulation and presented in Figure 17. The results confirm the insertion of the polar residues of all peptides into the membrane surface, with the hydrophobic residues remaining mostly on the outside of the membrane. The densities at the beginning and at the end of simulations do not show significant difference, however, TSO8_lin and TSO8(3-39) seem to enter slightly deeper into the membrane than TSO8(1-39). The number of contacts between the P atoms of the membrane lipids and the polar and hydrophobic residues of the peptides were also calculated during the 1.5 μs simulation time. The results presented in Figure 18 again prove that the interaction between the membrane and the peptides is electrostatic, as the count of the polar residue contacts with the membrane is far higher than the one for the hydrophobic residues. Among the peptides, TSO8(1-39) has the lowest count of contacts with the membrane during the simulation, which was expected due to its C-terminal segment remaining on the outside for the 1.5 μs simulation time.

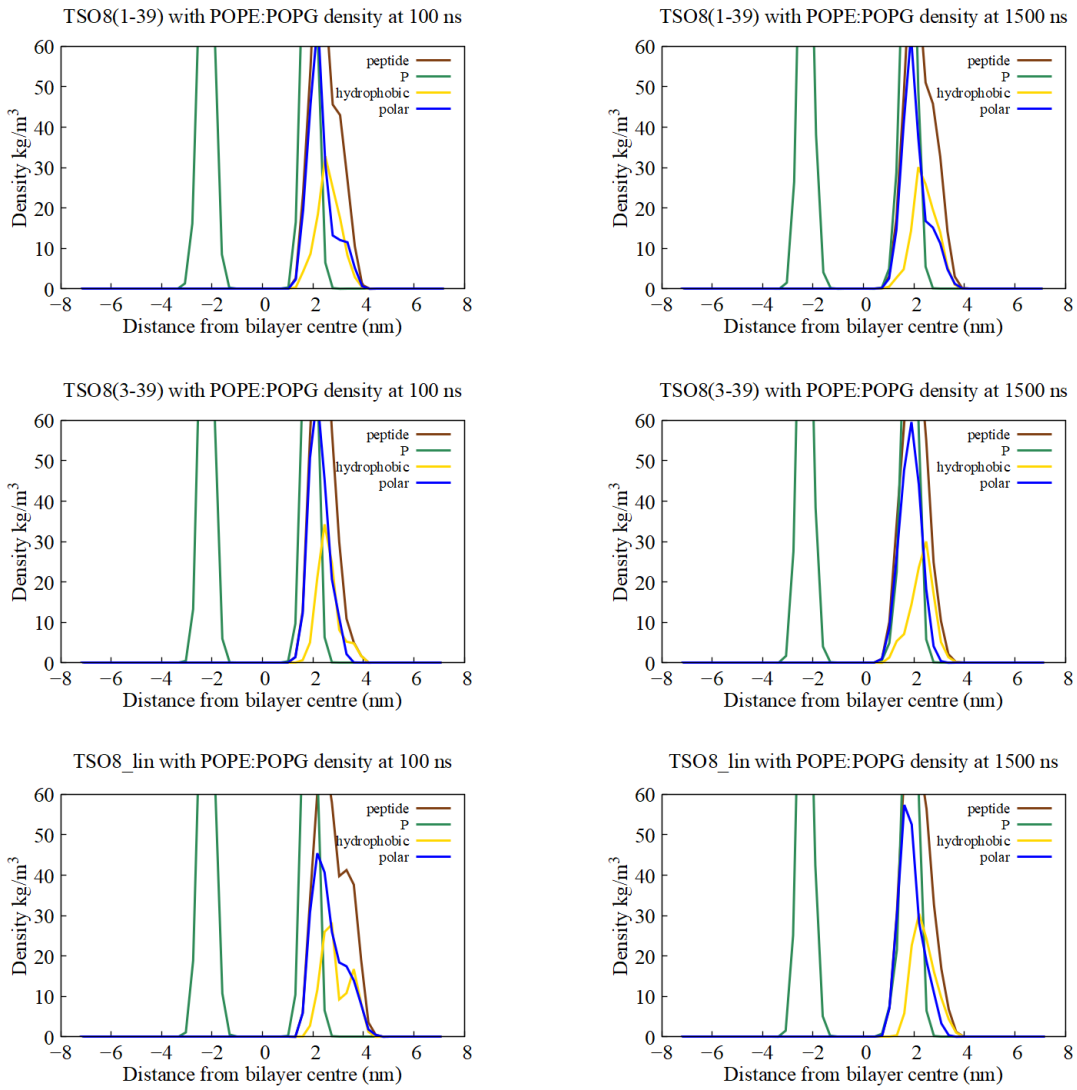

Figure 17 Density profiles averaged at t=100 ns (left) and t=1.5 μs (right), calculated for P atoms of membrane lipids as well as polar (blue) and hydrophobic (yellow) residues of TSO8(1-39) (top), TSO8(3-39) (middle) and TSO8_lin (bottom).

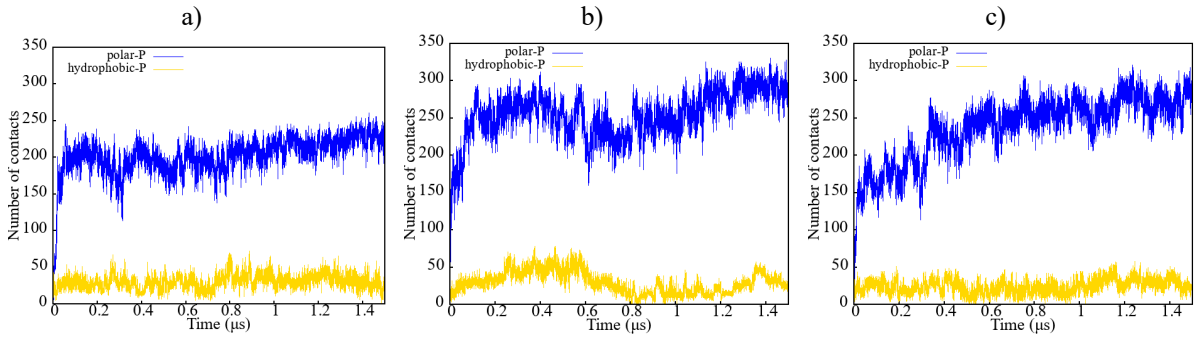

Figure 18 Number of contacts between P atoms of membrane lipids and hydrophobic (yellow) and polar (blue) residues calculated for: a) TSO8(1-39), b) TSO8(3-39) and c) TSO8_lin.

To examine the interaction of peptide with the membrane in more details, the densities were calculated separately for N-terminal α-helix, which includes the first 19, or in the case of TSO8(3-39), the first 17 residues and C-terminal coil which includes the rest of the residues. The results are presented in Figure 19. In each case shifting of the helical part towards the membrane centre during simulations time is observed, however helices remain in the polar region.

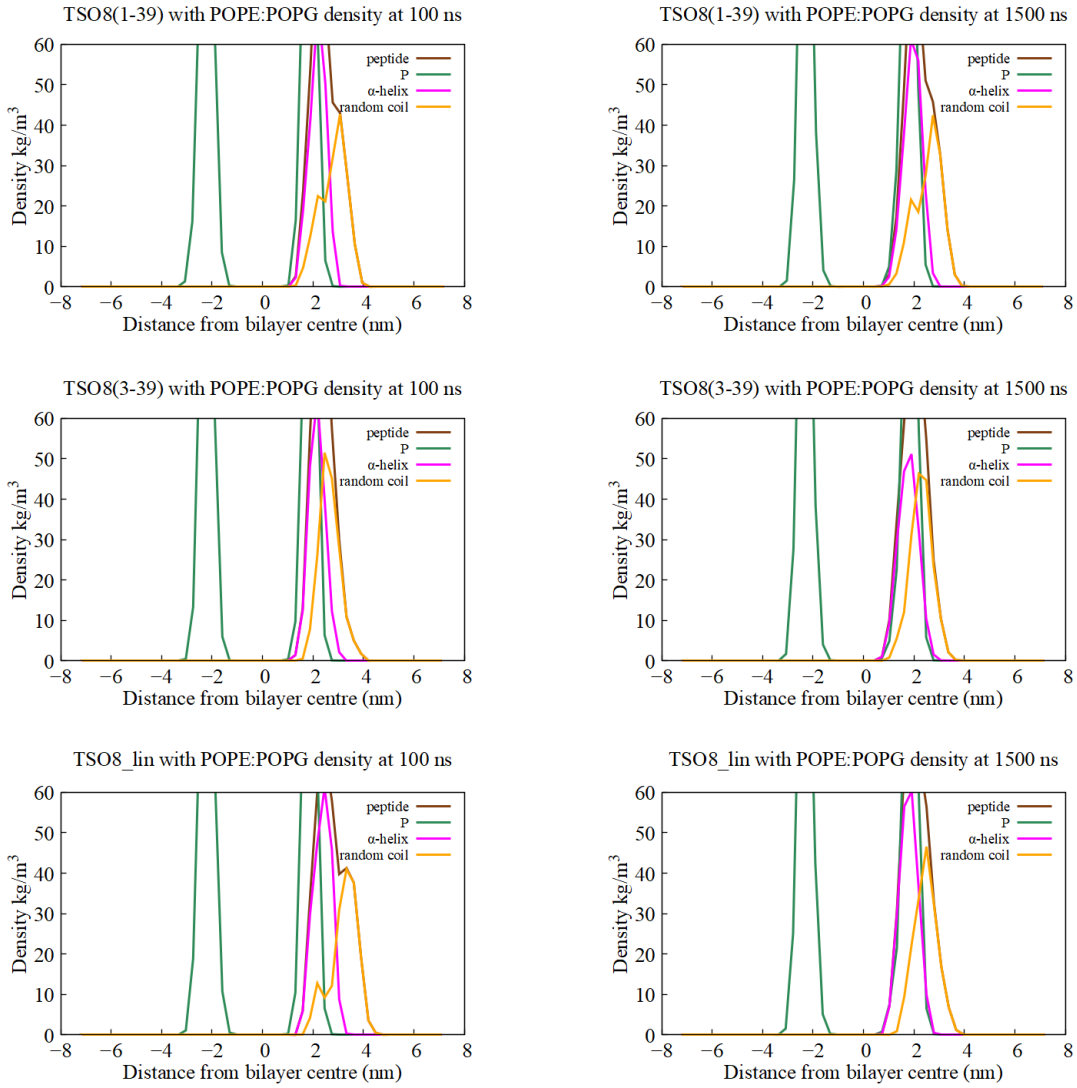

Figure 19 Density profiles averaged at t=100 ns (left) and t=1.5 μs (right), calculated for P atoms of membrane lipids as well as N-terminal α-helix (magenta) and C-terminal coil (orange) residues of: of TSO8(1-39) (top), TSO8(3-39) (middle) and TSO8_lin (bottom).

Finally, the results of DSSP secondary structure are presented in Figure 20. The persistence of the N-terminal α-helix during the 1.5 μs simulation time is observed in each case, with TSO8(3-39) exhibiting some structural changes of the first 8 residues within the first 500 ns of the simulation. The C-terminal segments of each peptide retain their unstructured nature during the simulation time, showing no signs of developing alternative structural motifs, such as β-sheets observed in the case of TSO8_lin in water.

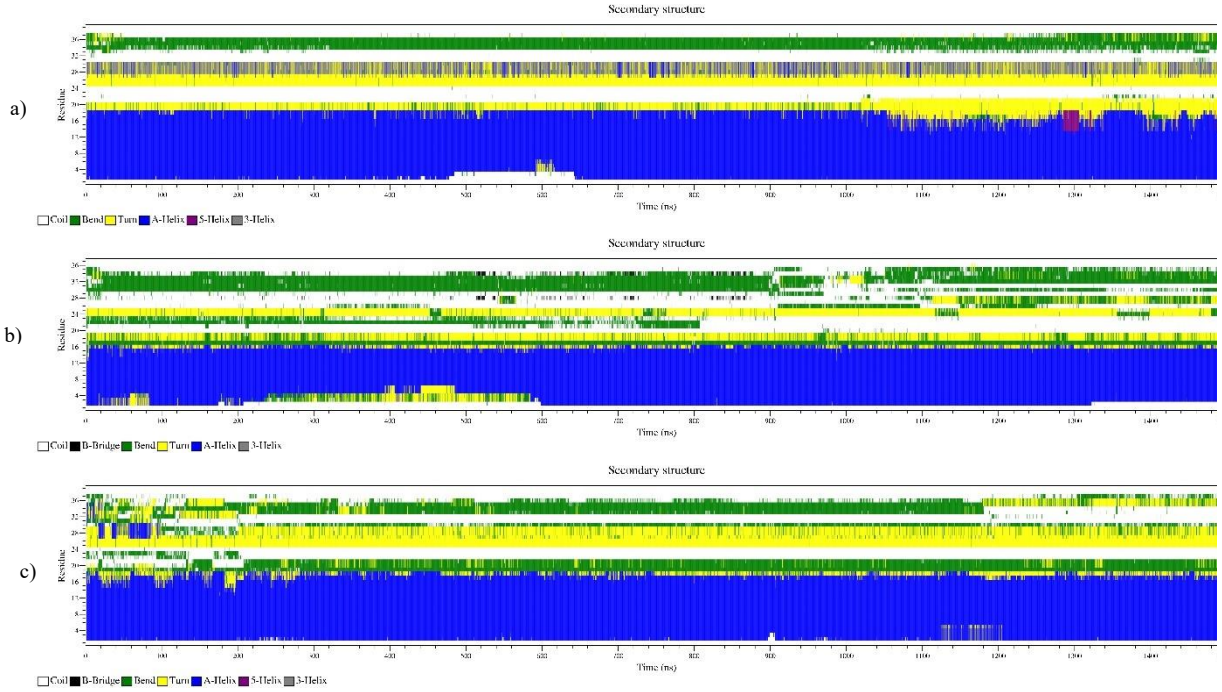

Figure 20 DSSP analysis for peptides throughout the 1.5 μs long simulations with POPE : POPG membrane: a) TSO8(1-39), b) TSO8(3-39) and c) TSO8_lin.

5.2.2 Short peptides near the membrane

To analyse the interaction of shorter fragments with the membrane TSO8(1-23), TSO8(3-23) and TSO8(20-39) each underwent 1 μs long simulations. Initial positions of the peptides presented in Figure 21 were again as described in section 5.2.1. The behaviour of both N-terminal fragments TSO8(1-23) and TSO8(3-23) is similar to that observed in long peptides. The α-helix swiftly contacts the membrane with its polar residues, while the hydrophobic residues remain on the exterior. However, while the majority of the α-helix remains stable for both of these fragments, the ends of the peptides exhibit unfolding, which is confirmed both by visual inspection and by the DSSP analysis presented in Figure 29. Again, the α-helical segment of the peptides remains in the polar region throughout the 1 μs simulation, however, the insertion of the unfolded fractions of both peptides deeper into the membrane is observed. On the other hand, the C-terminal unstructured fragment TOS8(20-39) showcases a completely different interaction with the membrane, exhibiting very low affinity for membrane binding.

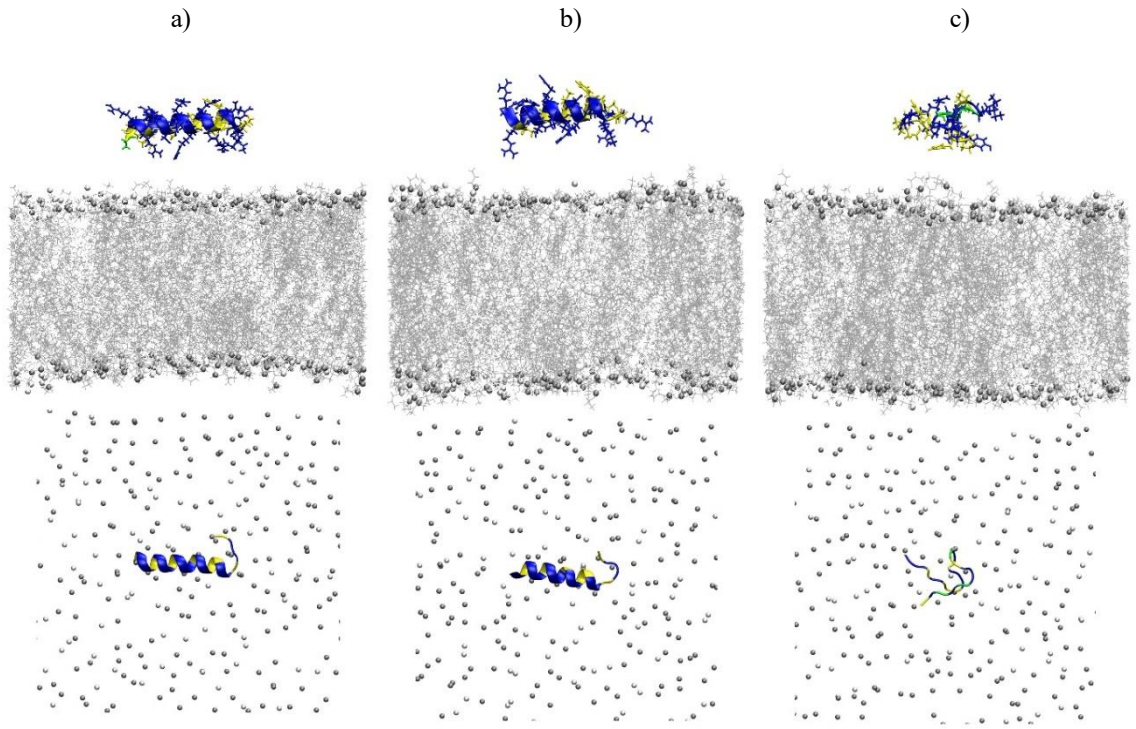

Figure 21 Initial states of peptides near the POPE:POPG membrane model as seen from the side (top) and top (bottom) for: a) TSO8(1-23), b) TSO8(3-23) and c) TSO8(20-39). Amino acids are coloured according to their hydrophobicity (polar – blue, hydrophobic – yellow, glycine - green). Membrane is coloured by residue name (POPE – silver, POPG - white). Water molecules and ions are not shown for clarity.

Figure 22 illustrates the interaction of TSO8(1-23) with the membrane during the 1 μs simulation time. It is evident that the short unstructured segment at the C-terminal of TSO8(1-23) enters the membrane with the hydrophobic residue. This might be the first step towards the hydrophobic insertion, which the shorter fragments could potentially exhibit.

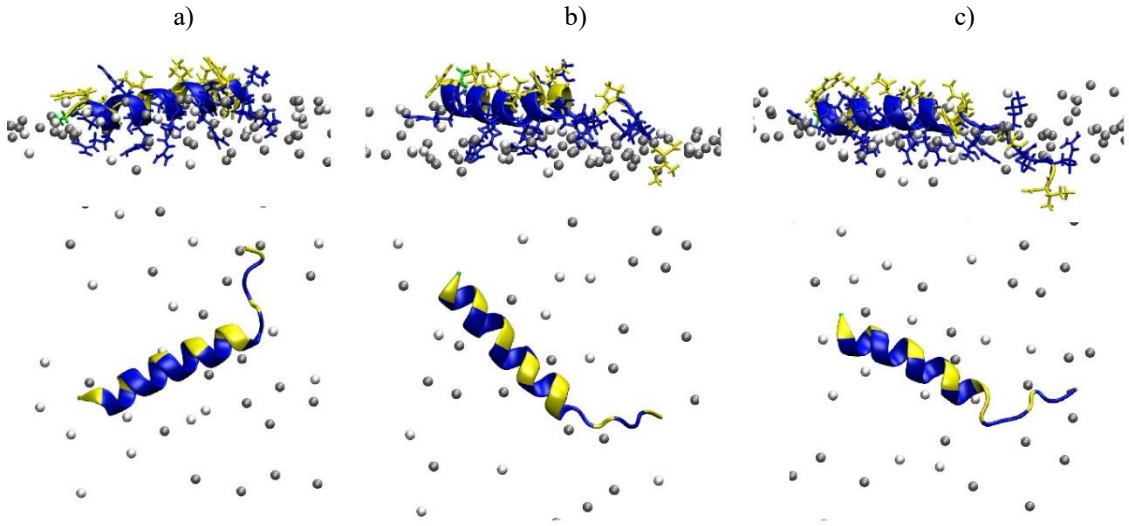

Figure 22 Snapshots from 1 μs long simulation of TSO8(1-23) near the POPE:POPG membrane. Side (top) and top (bottom) view of peptide states at times a) t=100 ns, b) t= 500 ns and c) t =1 μs. Amino acids are coloured according to their hydrophobicity (polar – blue, hydrophobic – yellow, glycine - green). Membrane is represented only by P atoms of the upper leaflet (POPE – silver, POPG - white). Water molecules and ions are not shown for clarity.

Figure 23 depicts the behaviour of TSO8(3-23) during the simulation time of 1 μs with the membrane. Again, the insertion of the hydrophobic residue at the C-terminal into the membrane layer is shown.

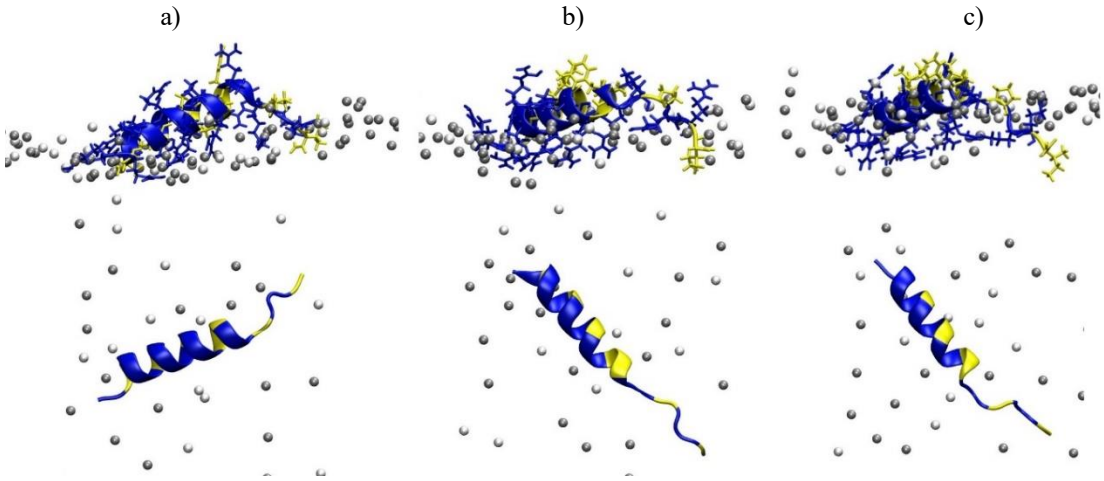

Figure 23 Snapshots from 1 μs long simulation of TSO8(3-23) near the POPE:POPG membrane. Side (top) and top (bottom) view of peptide states at times a) t=100 ns, b) t= 500 ns and c) t =1 μs. Amino acids are coloured according to their hydrophobicity (polar – blue, hydrophobic – yellow, glycine - green). Membrane is represented only by P atoms of the upper leaflet (POPE – silver, POPG - white). Water molecules and ions are not shown for clarity.

Finally, Figure 24 illustrates the interaction of the C-terminal short fragment TSO8(20-39) with the membrane during the 1 μs simulation. This fragment exhibits completely different behaviour than previously seen in all other fragments. It contacts the membrane only with a few of its residues and shows no insertion even in the polar region of the membrane after 1 μs. This is strong evidence that the α-helix structure of the TSO8 peptide is crucial for the peptide contact with the membrane.

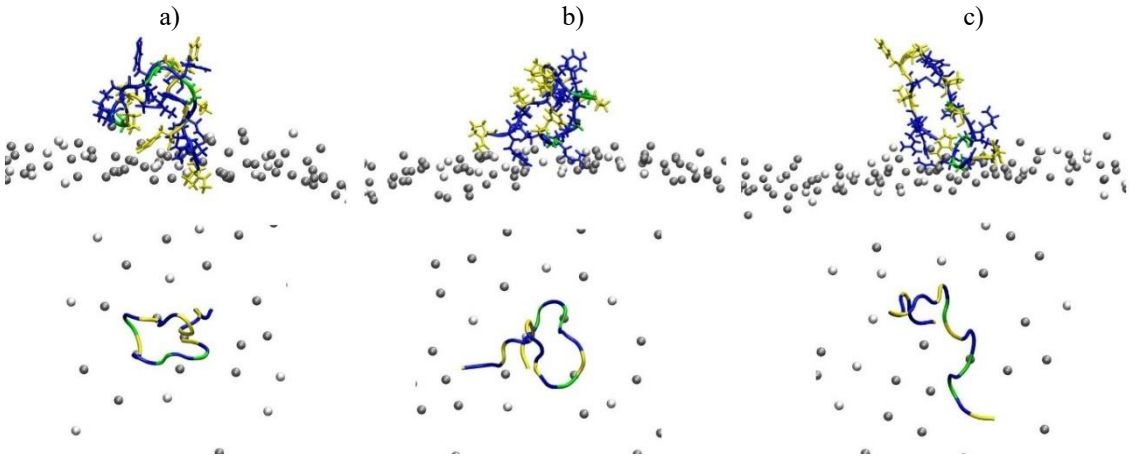

Figure 24 Snapshots from 1 μs long simulation of TSO8(20-39) near the POPE:POPG membrane. Side (top) and top (bottom) view of peptide states at times a) t=100 ns, b) t= 500 ns and c) t =1 μs. Amino acids are coloured according to their hydrophobicity (polar – blue, hydrophobic – yellow, glycine - green). Membrane is represented only by P atoms of the upper leaflet (POPE – silver, POPG - white). Water molecules and ions are not shown for clarity.

The 3DHMs and the electrostatic potential maps at the peptide surface, were calculated for the initial and final (1 μs) configurations of short peptides. The results demonstrate a similar trend to that observed for long peptides, with the 3DHM values increasing over the course of the simulation. However, the results once again confirm that the peptides remain within the polar region of the membrane, as indicated by the orientation of the vector, which points away from the membrane surface. TSO8(1-23) exhibits lower values of 3DHM at both moments, as well as a smaller angle between the 3DHM vector and z axes, compared to TSO8(3-23).

Table 5.2 Absolute values of 3DHM calculated for the initial and final (t=1μs) configurations of TSO8(1-23), TSO8(3-23) and TSO8(20-39) for simulations near the membrane. The results were obtained using two different dielectric constants: for the initial position of the peptide in water, dielectric constant was 78.5, while for the final position of the peptide at the interface of membrane and water the dielectric constant was 20.0 [15].

Peptide	3DHM at t=0 ns [AkT/e]	3DHM at t=1.5 μs [AkT/e]
TSO8(1-23)	9.724	59.185
TSO8(3-23)	18.821	88.237
TSO8(20-39)	6.096	27.665

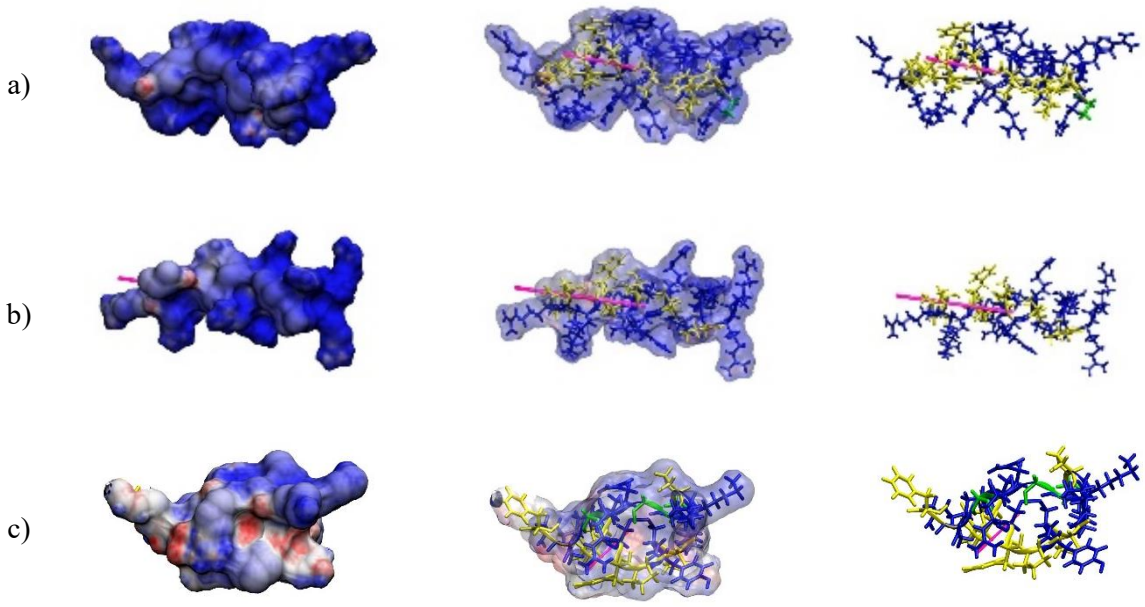

Figure 25 3DHM calculations where the electrostatic potential map of the peptide surface is shown on the left (opaque) and in the middle (transparent), and peptide structure with the 3DHM vector is shown on the right for: a) TSO8(1-23), b) TSO8(3-23) and c) TSO8(20-39) at the initial time of the simulations with POPE:POPG membrane (not shown for clarity). Peptides are parallel to the membrane surface. Hydrophobic residues are coloured yellow, polar residues blue and glycine residues green. 3DHM vector is coloured magenta. Positively charged regions of the electrostatic potential are coloured blue, and negatively charged regions are coloured red.

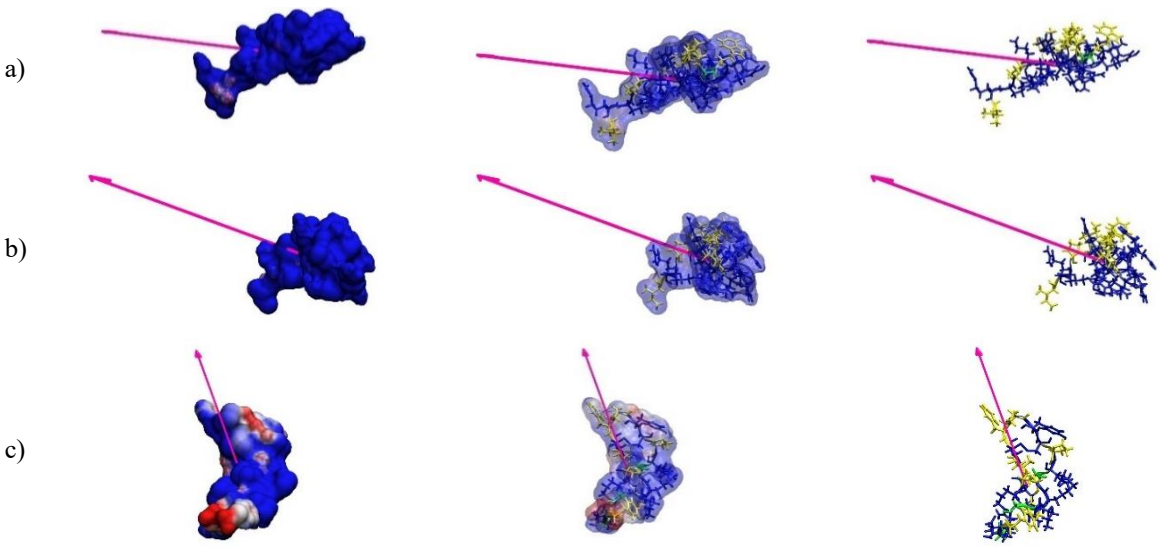

Figure 26 3DHM calculations where the electrostatic potential map of the peptide surface is shown on the left (opaque) and in the middle (transparent), and peptide structure with the 3DHM vector is shown on the right for: a) TSO8(1-23), b) TSO8(3-23) and c) TSO8(20-39) at the final (1 μs) time of the simulations with POPE:POPG membrane (not shown for clarity). Peptides are parallel to the membrane surface. Hydrophobic residues are coloured yellow, polar residues blue and glycine residues green. 3DHM vector is coloured magenta. Positively charged regions of the electrostatic potential are coloured blue, and negatively charged regions are coloured red.

To further examine the behaviour of hydrophobic and polar residues during the simulations, density profiles were calculated, as average for the first and last 100 ns of the simulation. The results presented in Figure 27 confirm that both TSO8(1-23) and TSO8(3-23) exhibit similar behaviour to the one observed for long peptides. The polar residues shift towards the membrane centre during the simulation, while the hydrophobic residues remain on the outside, again confirming the electrostatic nature of the peptide-membrane interaction. Additionally, the results suggest that TSO8(20-39) also binds to the membrane surface, however the majority of the peptide remains positioned on the exterior. These observations are confirmed by the calculation of the number of contacts between the P atoms of the membrane lipids and the polar and hydrophobic residues of the peptides, presented in Figure 28. Both TSO8(1-23) and TSO8(3-23) show similar behaviour, with polar residues making more contacts with the membrane throughout the simulation than the hydrophobic residues, while TOS8(20-39) shows very few contacts of both regions compared to the rest of the peptides.

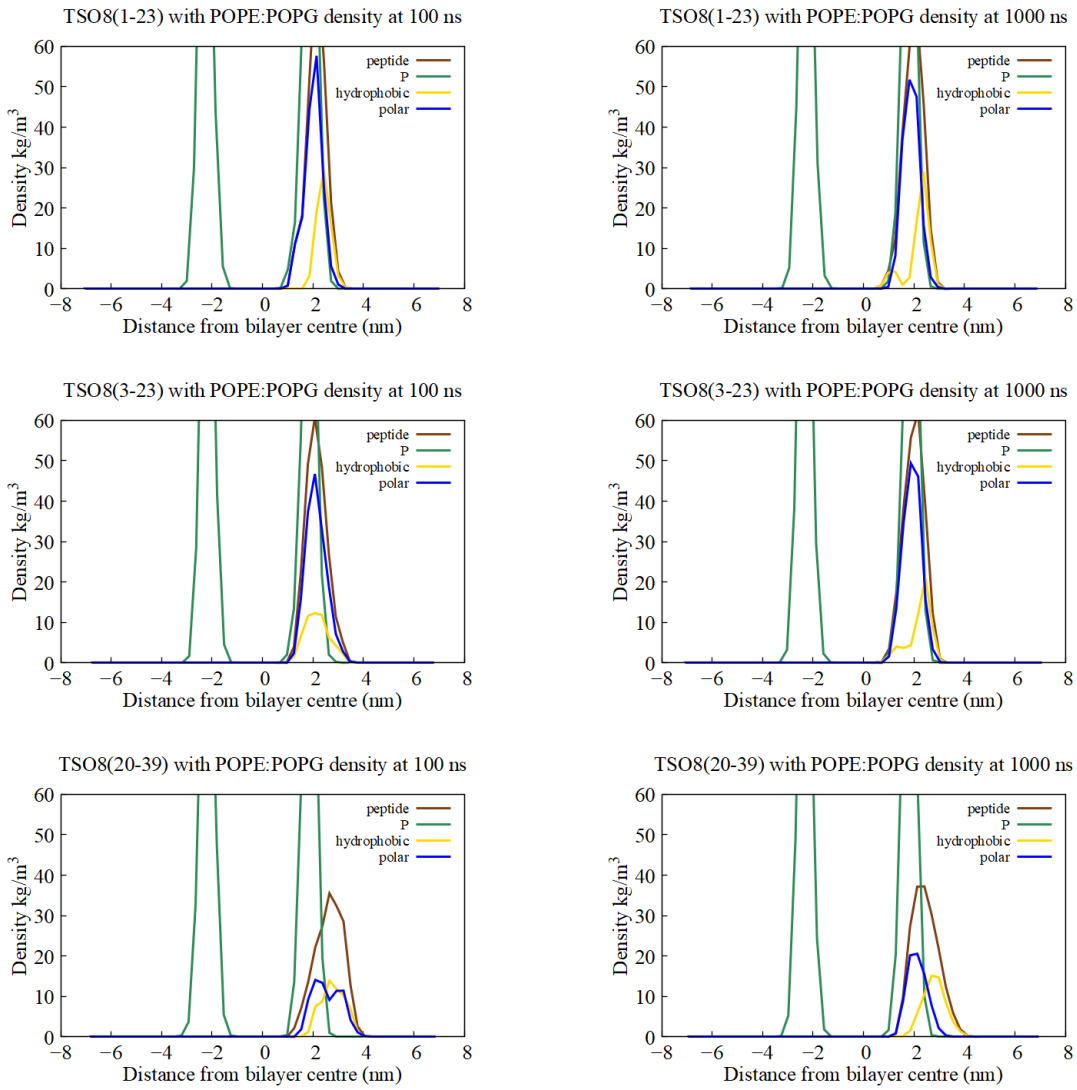

Figure 27 Density profiles averaged at t=100 ns (left) and t=1 μs (right), calculated for P atoms of membrane lipids as well as polar (blue) and hydrophobic (yellow) residues of: TSO8(1-23) (top), TSO8(3-23) (middle) and TSO8(20-39) (bottom).

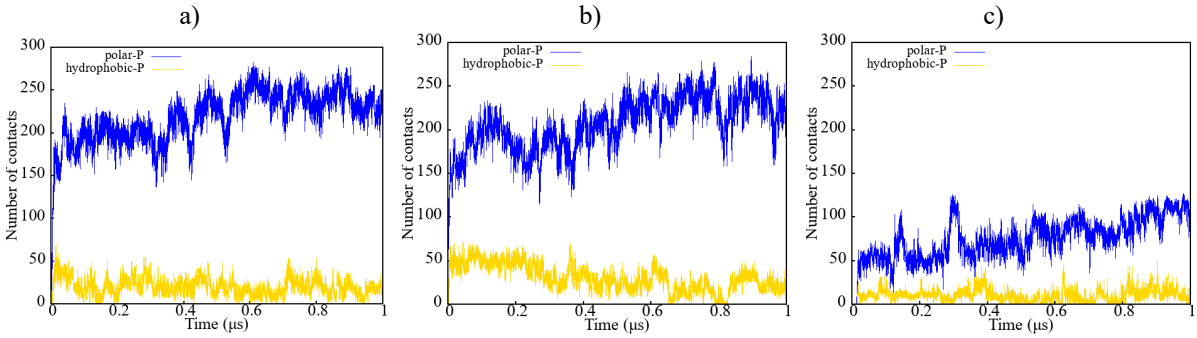

Figure 28 Number of contacts between P atoms of membrane lipids and hydrophobic (yellow) and polar (blue) residues calculated for a) TSO8(1-23), b) TSO8(3-23) and c) TSO8(20-39).

Structural analysis was again done for short fragments and presented in Figure 29. The α-helical segments of both TSO8(1-23) and TSO8(3-23) exhibit more structural changes during the 1 μs simulation time, compared to the longer fragments, but are still mostly preserved.

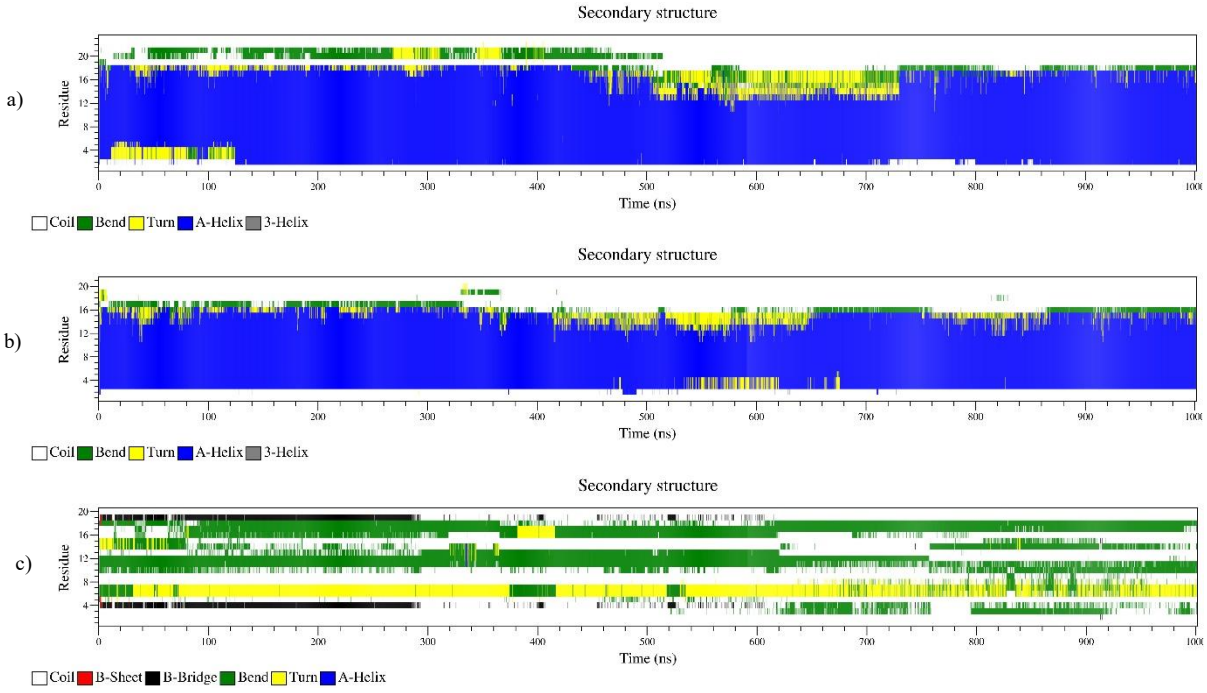

Figure 29 DSSP analysis for peptides throughout the 1 μs long simulations with POPE:POPG membrane: (a) TSO8(1-23), (b) TSO8(3-23) and (c) TSO8(20-39).

5.2.3 Summary of the results for single peptides near the membrane

Simulations of peptides interacting with membrane were performed to examine the mode of action, and roles of different specific segments of the TSO8 peptide. It is evident that the first step in peptide membrane interaction is α-helix insertion into the polar region of the membrane, where they remain during the simulation. It is important to emphasize that TSO8 is a natural AMP with a more complex structure than most of designed AMPs whose structure is purely α-helical. Therefore, the dynamics of the peptide membrane interaction are probably more complicated, or in the least a lot slower. The shorter fragments seem to exhibit a faster process of insertion, which is to be expected of a mostly α-helical structure, but is not in line with the experimental data (see Table 4.2 and Figure 4) where the shorter fragments showed less potency and toxicity compared to the longer ones. This inconsistency might stem from the fact the experimental results of the peptide activity depend much more on the further steps in the peptides mode of action, while this work only observes the first contacts with the membrane. The C-terminal coil has very low affinity for interaction with the membrane, and its role could not be determined with certainty. It is possible, considering its proline content, that its role in nature is to protect the helical segment of the peptide against certain proteases [57]. Similar could possibly be assumed for the role of the disulfide bridge, though the disulfide bridge loop in TSO8 is notably smaller than those previously reported to be serine protease inhibitors [58].

5.3 Investigation of associations

Several systems containing multiple TSO8(1-39) peptides were analysed to investigate their tendency to cluster. The initial experiment involved a system containing twelve TSO8(1-39) peptides in water. Additionally, the behaviour of multiple peptides in the vicinity of the membrane was tested through three different simulations. The first simulation involved twelve TSO8(1-39) peptides, while the second and third simulations involved six peptides each, conducted at different temperatures.

5.3.1 Multiple TSO8(1-39) peptides in water

The experimental results suggested that peptides show strong affinity for associations in water. Therefore, a simulation of twelve TSO8(1-39) peptides in water was performed in this work. The visual inspection of the simulation dynamics showed that initially separated peptides, illustrated in Figure 30 on the left, associate rapidly and at the end of simulation (t=1.5 μs), shown in Figure 30 on the right, form one large cluster.

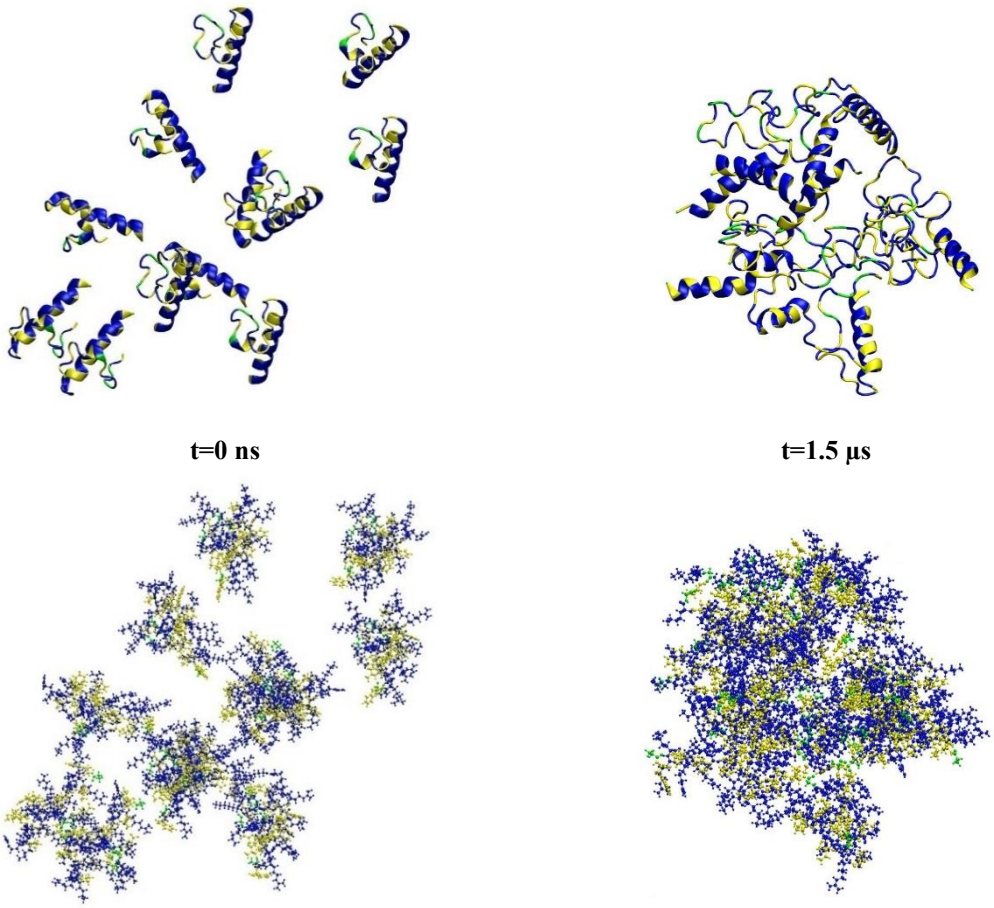

Figure 30 Initial (left) and final (right) states of twelve TSO8(1-39) after 1.5 μs simulation in water. Amino acids are coloured according to their hydrophobicity (polar – blue, hydrophobic – yellow, glycine - green). Peptides are shown in two representations: secondary structure representation (top) shows the stability of α-helices, while sticks and balls representation shows all atoms in the peptide for a better understanding of the clustering. Water molecules and ions are not shown for clarity.

Cluster size distribution, presented in Figure 31 on the left, indicates that the most favourable configuration of the system, during the 1.5 μs long simulation, is a cluster containing all twelve peptides. This is supported by the cluster count presented in Figure 31 on the right, where it can be seen that all peptides form one cluster after 1.0 μs simulation time, which remains stable for the rest of the simulation. These results demonstrate the high affinity of peptide associations in water.

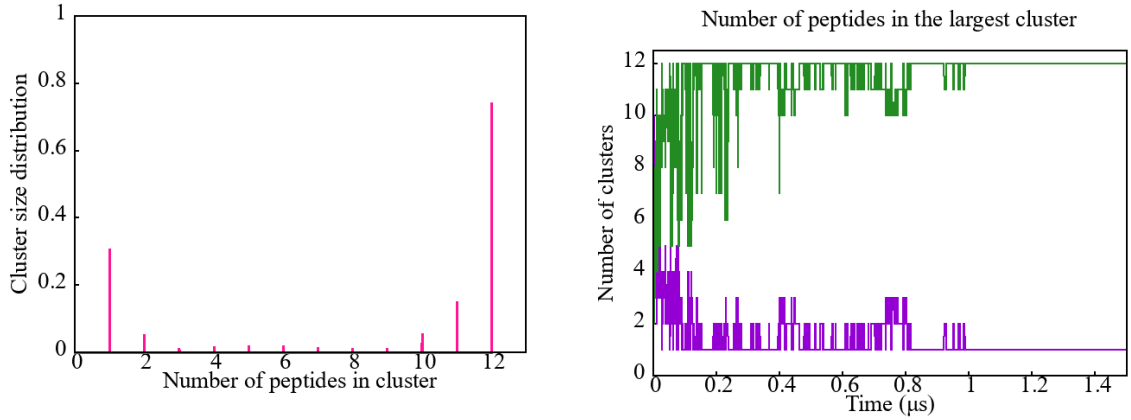

Figure 31 Cluster size distribution (left) and the number of clusters as a function of time (right) calculated for the 1.5 μs long simulation of twelve TSO8(1-39) peptides in water. The number of clusters is coloured violet, while the number of peptides in the largest cluster is coloured green.

5.3.2 Multiple TSO8(1-39) peptides in the vicinity of the membrane

To investigate the association of peptides on the membrane surface, and the role of associations in their mode of action, multiple TSO8(1-39) peptides were placed in the vicinity of the membrane, which consisted of a total of 592 lipids.

Initially, twelve TSO8(1-39) peptides were examined through a 700 ns long simulation. The challenges related to this system are described in detail in section 8.2 of the Appendix. The initial and final states of this system are illustrated in Figure 32 and Figure 33 respectively. The visual inspection confirms that peptides once again stay in the polar region of the membrane, with no observed hydrophobic insertion, as was the case for single peptides.

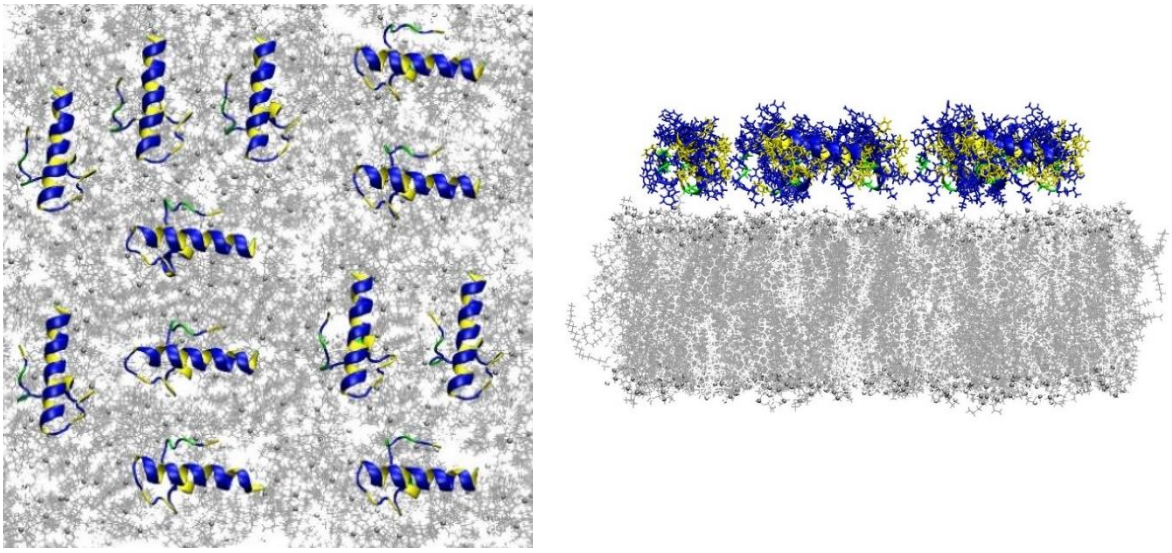

Figure 32 Initial state of twelve TSO8(1-39) peptides in the vicinity of POPE:POPG membrane as seen from the top (left) and side (right). Amino acids are coloured according to their hydrophobicity (polar – blue, hydrophobic – yellow, glycine - green). Membrane is coloured by residue name (POPE – silver, POPG - white). Water molecules and ions are not shown for clarity.

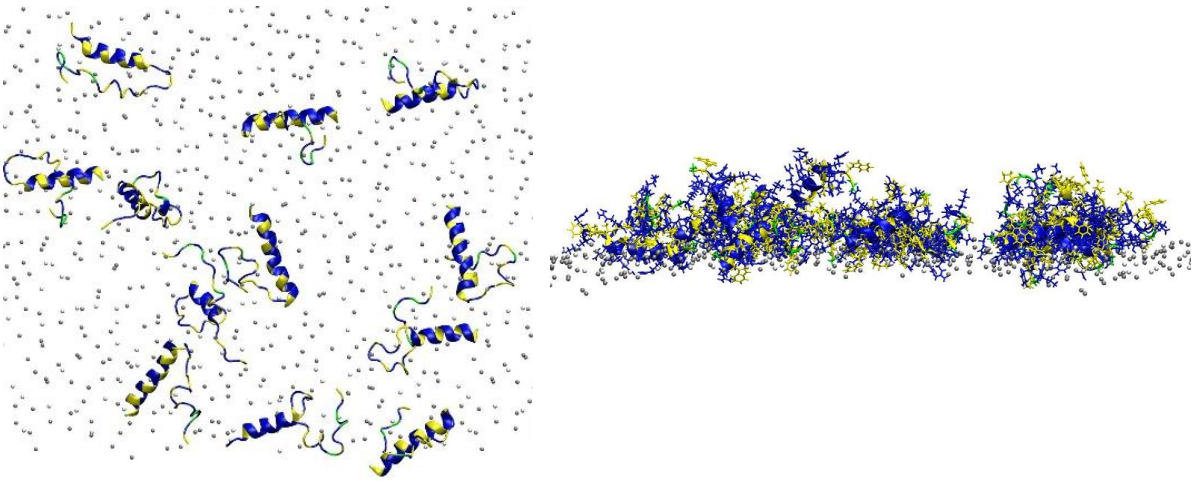

Figure 33 Final state (t=700 ns) of twelve TSO8(1-39) peptides in the vicinity of POPE:POPG membrane as seen from the top (left) and side (right). Amino acids are coloured according to their hydrophobicity (polar – blue, hydrophobic – yellow, glycine - green). Membrane is represented only by P atoms of the upper leaflet (POPE – silver, POPG - white). Water molecules and ions are not shown for clarity.

The cluster size distribution, presented in Figure 34 on the left, indicates a significant preference for clusters containing single peptides during the 700 ns simulation time. Nonetheless, several clusters comprising multiple peptides have also been observed. This variety in cluster size and number of clusters is also demonstrated by the results in Figure 34 on the right. While certain clustering is evident for this simulation time of twelve peptides, it is not conclusive whether it arises from the peptides' inherent tendency to associate on the membrane surface or from the high concentration of the peptides near the membrane.

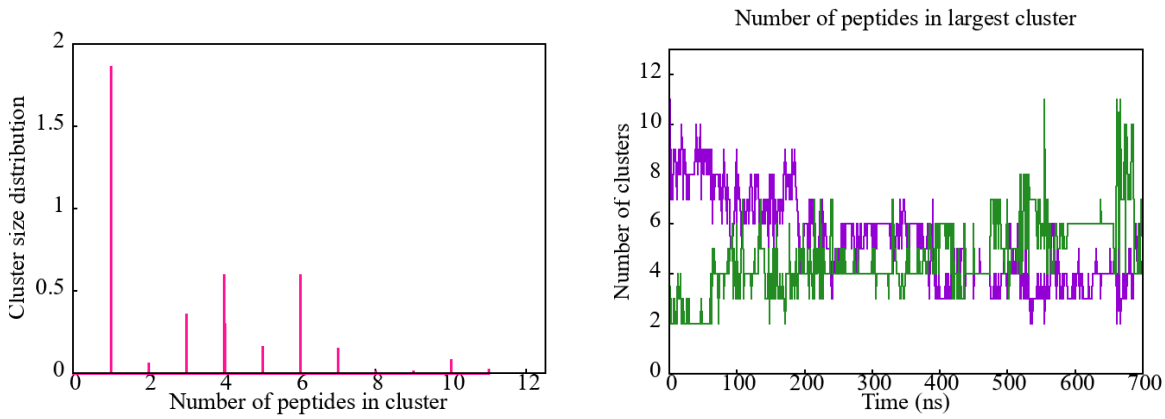

Figure 34 Cluster size distribution (left) and the number of clusters as a function of time (right) calculated for the 700 ns long simulation of twelve TSO8(1-39) peptides in the vicinity of POPE:POPG membrane. The number of clusters is coloured violet, while the number of peptides in the largest cluster is coloured green.

To address the uncertainty stemming from these results, a system containing the reduced number of peptides was investigated. For the next experiment, six peptides were placed near the same membrane model, containing 592 lipids, and underwent a 1 μs long simulation. The initial and final states of this system are depicted in Figure 35 and Figure 36 respectively.

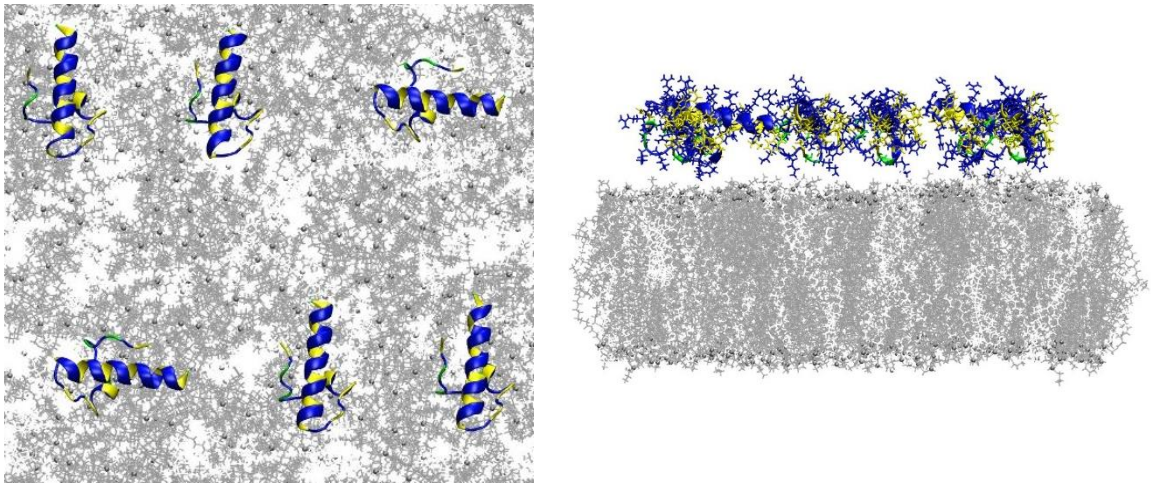

Figure 35 Initial state of six TSO8(1-39) peptides in the vicinity of POPE:POPG membrane, at the temperature of 310 K, as seen from the top (left) and side (right). Amino acids are coloured according to their hydrophobicity (polar – blue, hydrophobic – yellow, glycine - green). Membrane is coloured by residue name (POPE – silver, POPG - white). Water molecules and ions are not shown for clarity.

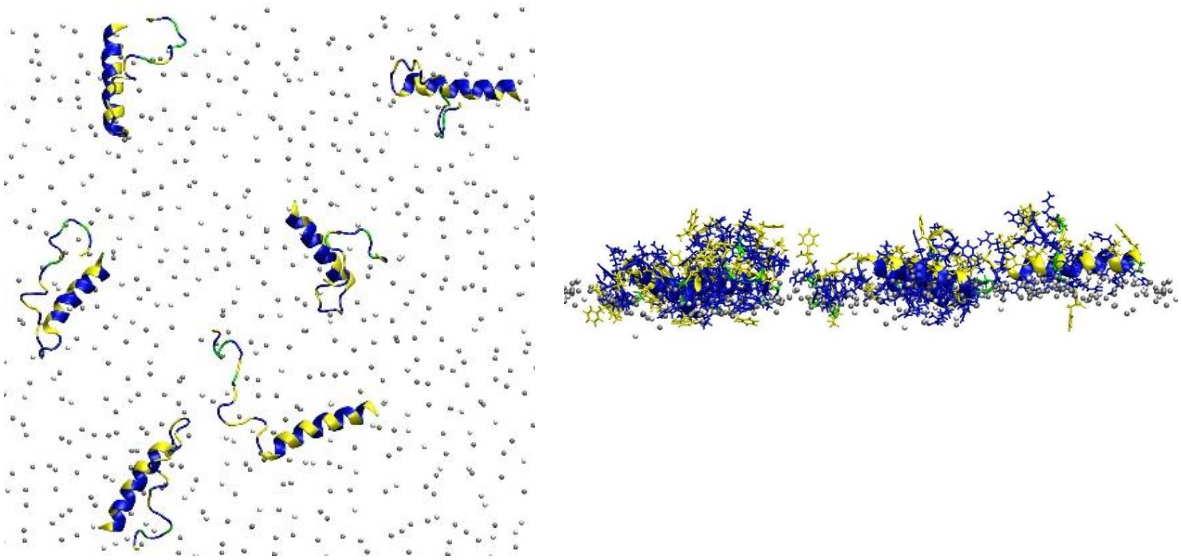

Figure 36 Final state (t=1 μs) of six TSO8(1-39) peptides in the vicinity of POPE:POPG membrane, at the temperature of 310 K, as seen from the top (left) and side (right). Amino acids are coloured according to their hydrophobicity (polar – blue, hydrophobic – yellow, glycine - green). Membrane is represented only by P atoms of the upper leaflet (POPE – silver, POPG - white). Water molecules and ions are not shown.

Figure 37 on the left presents the results of cluster size distribution analysis for this system, which indicate the highest probability for single-peptide clusters, although clusters containing multiple peptides can also be observed. This is supported by the cluster count presented in Figure 37 on the right, where clusters containing two or three peptides are observed towards the end of the simulation. These results suggest two possible conclusions: either the peptides lack the tendency to associate on the membrane surface, or the dynamics of their association is slow enough that it cannot be observed within this simulation timeframe.

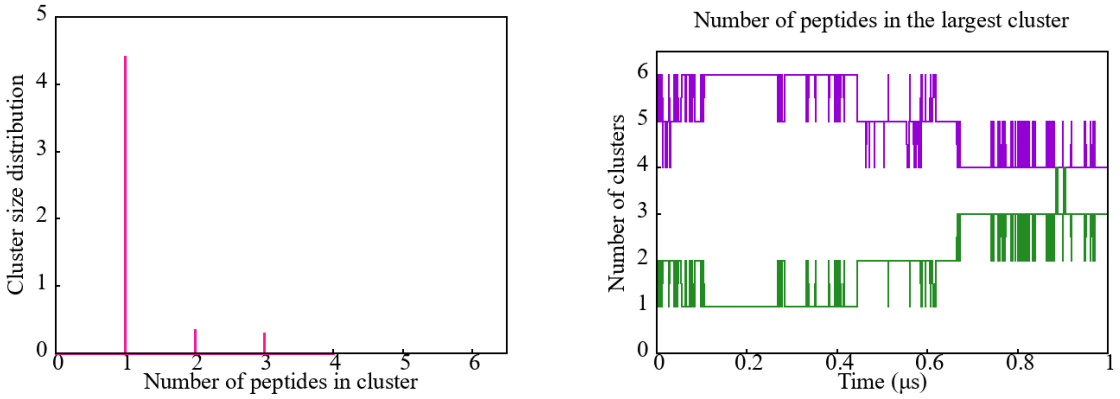

Figure 37 Cluster size distribution (left) and the number of clusters as a function of time (right) calculated for the 1 μ long simulation of six TSO8(1-39) peptides in the vicinity of POPE:POPG membrane, at the temperature of 310 K. The number of clusters is coloured violet, while the number of peptides in the largest cluster is coloured green.

Finally, the behaviour of the same system comprising of six peptides near the membrane was investigated at a higher temperature, specifically 380 K, for the same simulation duration (1 μs). As the increase in temperature amplifies the kinetic contributions, such a system should yield results indicating associations within a shorter simulation time, assuming the peptides do

have an inherent tendency to cluster. Figure 38 and Figure 39 illustrate the initial configuration of this system, and the one at the 1 μs simulation time, respectively. Visual inspection suggests that peptides in fact interact with the membrane separately and confirms that the peptides and the membrane are much less stable at higher temperatures.

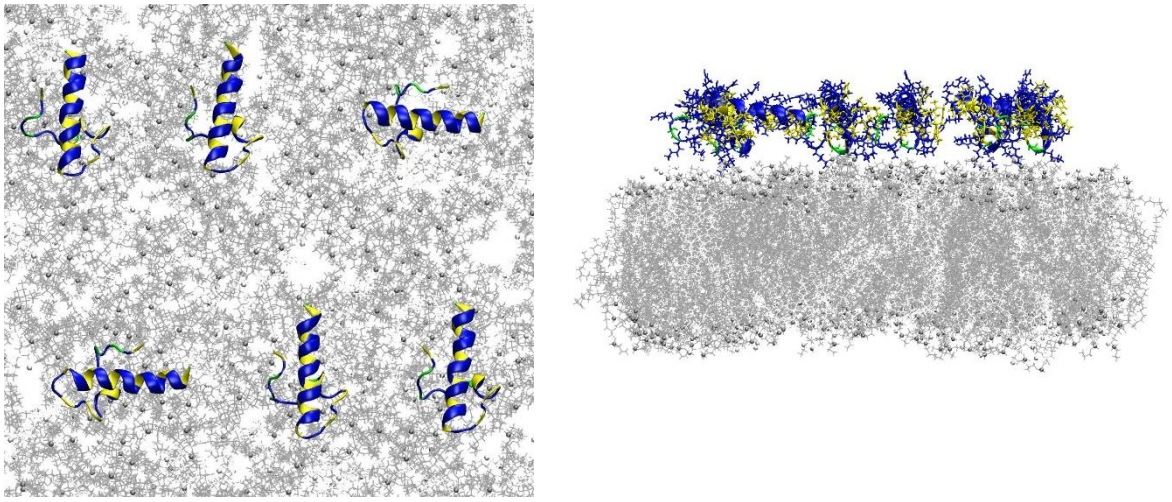

Figure 38 Initial state of six TSO8(1-39) peptides in the vicinity of POPE:POPG membrane, at the temperature of 380 K, as seen from the top (left) and side (right). Amino acids are coloured according to their hydrophobicity (polar – blue, hydrophobic – yellow, glycine - green). Membrane is coloured by residue name (POPE – silver, POPG - white). Water molecules and ions are not shown for clarity.

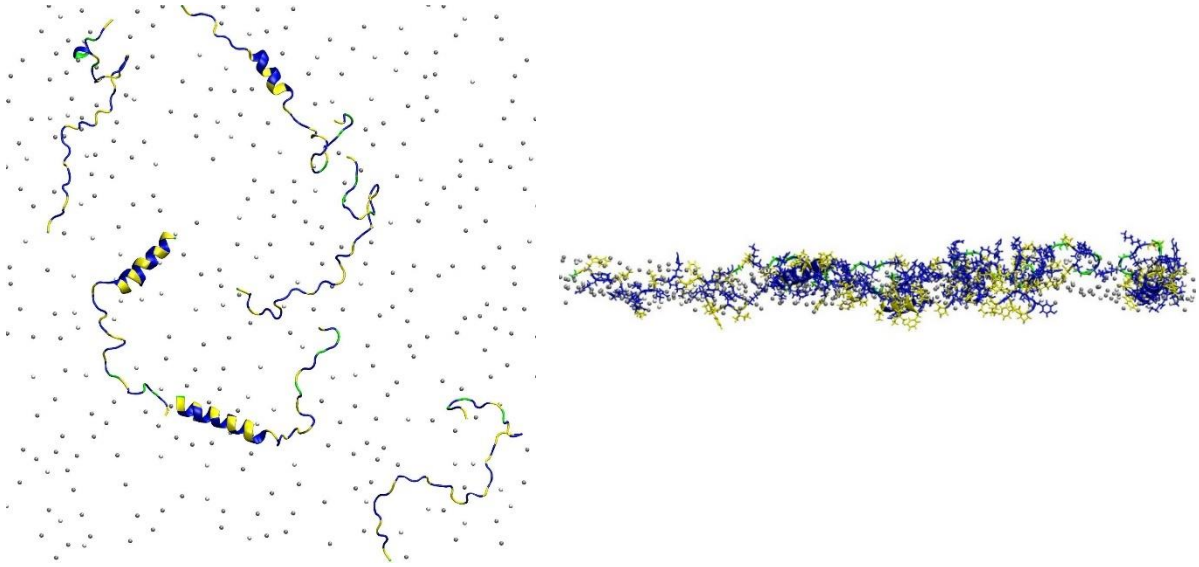

Figure 39 Final state (t=1 μs) of six TSO8(1-39) peptides in the vicinity of POPE:POPG membrane, at the temperature of 380 K, as seen from the top (left) and side (right). Amino acids are coloured according to their hydrophobicity (polar – blue, hydrophobic – yellow, glycine - green). Membrane is represented only by P atoms of the upper leaflet (POPE – silver, POPG - white). Water molecules and ions are not shown for clarity.

The results of the cluster analysis, depicted in Figure 40, again confirm that single-peptide clusters have the highest probability of forming, with several multi-peptide clusters also being observed. These results are similar to those previously obtained for the system at room temperature, suggesting consistent absence of clustering tendency of the TSO8(1-39) peptides.

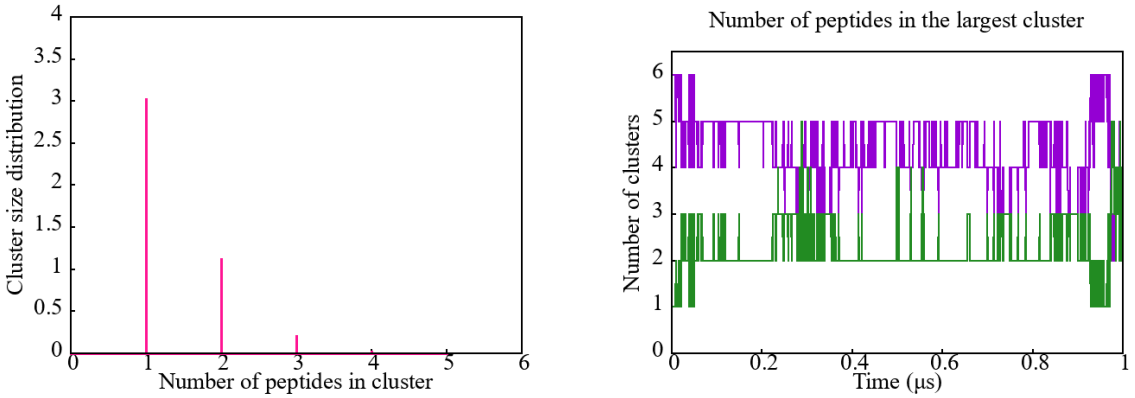

Figure 40 Cluster size distribution (left) and the number of clusters as a function of time (right) calculated for the 1 μ long simulation of six TSO8(1-39) peptides in the vicinity of POPE:POPG membrane, at the temperature of 380 K. The number of clusters is coloured violet, while the number of peptides in the largest cluster is coloured green.

5.3.3 Summary of the peptide association investigation

MD simulations were performed on systems containing multiple TSO8(1-39) peptides, both in water and in the vicinity of the membrane, aiming to explore their tendency to cluster. The results indicate a swift association of the peptides in water, forming a singular cluster. However, no significant clustering phenomenon was observed on the membrane surface. Given that experimental evidence suggests the importance of peptide associations in their mode of action, we may propose that the simulation timeframes attainable through the employed method may not be sufficient for detecting this phenomenon. AA simulations involving multiple peptides with the membrane are usually challenging, especially in the case of larger peptides such as the investigated TSO8, which require a construction of larger systems and consequently more resources than are readily available. Thus, it can be suggested that a simplified model, such as CG model, could be useful in achieving longer simulation times potentially required for the manifestation of significant clustering.

6 Conclusion

Antibacterial resistance remains a major problem in need of answering in recent decades. Antimicrobial peptides play an important role in the defence mechanism of almost all organism, and as such represent a promising alternative to classical antibiotic treatment. An area that has been underexplored is the study of AMPs produced by helminth parasites. Due to parasites' ability to adapt to different conditions, these peptides hold promise as potential novel drugs for combating infectious diseases, that could be effective without causing excessive toxicity. One such peptide is TSO8, identified in *T. solium*, which is the focus of this research. TSO8 peptide contains 39 amino acids, with a net charge of +15.9 at pH 7. It has a specific structure with its N-terminal being α-helical with initial GW sequence, and its C-terminal having a coil like structure containing a disulfide bridge. In previous works, the peptides antimicrobial activity has been tested and it proved to be potent against both Gram-negative and Gram-positive bacterial strains. To assess the atomistic details of its mode of action and the roles of its structural motifs, TSO8 peptide and its four specific fragments, along with a linearized peptide obtained by replacing cysteine residues with alanine, were investigated through molecular dynamics simulations in various environments.

Firstly, the results of simulations of single peptides in water, show definite evidence of the role of GW sequence in the stability of the α-helix, which is in line with previous works [31]. Next, fragments were examined through simulations in the vicinity of a membrane model. The GW role could not be determined in these simulations, as all initially helical fragments showed structural stability during the simulation time. The results, however, elucidated the crucial role of the α-helix, as in all cases the initial contact with the membrane was formed by the helical segment of the peptide. The simulations of the C-terminal fragment indicate lack of affinity for membrane; therefore, we may speculate that its role is not directly linked with the peptide insertion in the membrane, or at less not in the process of the initial binding. We may propose that its function could be in protecting the α-helical region in another phase of the peptides mode of action [57].

Additionally, the association of peptides was explored through simulations of multiple TSO8(1-39) peptides. Such simulation in water showed their affinity for swiftly interacting and forming a single cluster. On the other hand, simulations of several peptides in the vicinity of the membrane showed that the peptides bind to the membrane surface individually, without an observable affinity for cluster formation. Moreover, peptides do not associate on the membrane even at higher temperatures and stay in the polar region of the membrane even for long simulation times.

The results of this work offer an atomistic insight which underscores several important aspects on the TSO8 peptide structural characterization and its mode of action. However, some results could not be obtained through the employed method of MD simulations with AA models, and we propose that further computational investigations should focus on a simplified model to facilitate longer simulation times with less difficulty, or even employ a new method of steered MD. Nonetheless, the findings of this work provide a solid foundation for ongoing biological and biophysical research promising fresh insight into the mode of action of TSO8 and similar helminth antimicrobial peptides.

7 Literature

1. Sakai, T. and Y. Morimoto, *The History of Infectious Diseases and Medicine.* Pathogens, 2022. **11**(10).
2. Ventola, C.L., *The antibiotic resistance crisis: part 1: causes and threats.* P t, 2015. **40**(4): p. 277-83.
3. Sengupta, S., M.K. Chattopadhyay, and H.P. Grossart, *The multifaceted roles of antibiotics and antibiotic resistance in nature.* Front Microbiol, 2013. **4**: p. 47.
4. Rončević, T., J. Puizina, and A. Tossi, *Antimicrobial Peptides as Anti-Infective Agents in Pre-Post-Antibiotic Era?* Int J Mol Sci, 2019. **20**(22).
5. Bin Hafeez, A., et al., *Antimicrobial Peptides: An Update on Classifications and Databases.* Int J Mol Sci, 2021. **22**(21).
6. Mahlapuu, M., et al., *Antimicrobial Peptides: An Emerging Category of Therapeutic Agents.* Front Cell Infect Microbiol, 2016. **6**: p. 194.
7. Pasupuleti, M., A. Schmidtchen, and M. Malmsten, *Antimicrobial peptides: key components of the innate immune system.* Crit Rev Biotechnol, 2012. **32**(2): p. 143-71.
8. *$CAMP_{R4}$: Collection of Anti-Microbial Peptides*. Available from: http://www.camp.bicnirrh.res.in/contactUs.php.
9. Gawde, U., et al., *CAMPR4: a database of natural and synthetic antimicrobial peptides.* Nucleic Acids Res, 2023. **51**(D1): p. D377-D383.
10. Rončević, T., et al., *Selection and redesign for high selectivity of membrane-active antimicrobial peptides from a dedicated sequence/function database.* Biochim Biophys Acta Biomembr, 2019. **1861**(4): p. 827-834.
11. Rončević, T., et al., *Antibacterial Activity Affected by the Conformational Flexibility in Glycine-Lysine Based α-Helical Antimicrobial Peptides.* J Med Chem, 2018. **61**(7): p. 2924-2936.
12. Cederlund, A., G.H. Gudmundsson, and B. Agerberth, *Antimicrobial peptides important in innate immunity.* Febs j, 2011. **278**(20): p. 3942-51.
13. Nijnik, A. and R. Hancock, *Host defence peptides: antimicrobial and immunomodulatory activity and potential applications for tackling antibiotic-resistant infections.* Emerg Health Threats J, 2009. **2**: p. e1.
14. Nguyen, L.T., E.F. Haney, and H.J. Vogel, *The expanding scope of antimicrobial peptide structures and their modes of action.* Trends Biotechnol, 2011. **29**(9): p. 464-72.
15. Maleš, M., *Different aspects of the mechanism of actions of antimicrobial peptides throughout simulation studies*, in *Prirodoslovno-matematički fakultet*. 2023, University of Split.
16. Brogden, K.A., *Antimicrobial peptides: pore formers or metabolic inhibitors in bacteria?* Nat Rev Microbiol, 2005. **3**(3): p. 238-50.
17. Rončević, T., et al., *Relating Molecular Dynamics Simulations to Functional Activity for Gly-Rich Membranolytic Helical Kiadin Peptides.* Pharmaceutics, 2023. **15**(5).
18. Čopac, R., *Synthesis, structural studies, molecular modeling and characterization of helminth antimicrobial peptides*, in *Faculty of Science*. 2022, University of Split.
19. Haney, E.F. and H.J. Vogel, *NMR of Antimicrobial Peptides*, in *Annual Reports on Nmr Spectroscopy, Vol 65*, G.A. Webb, Editor. 2009. p. 1-51.
20. Rončević, T., et al., *Anisaxins, helical antimicrobial peptides from marine parasites, kill resistant bacteria by lipid extraction and membrane disruption.* Acta Biomaterialia, 2022. **146**: p. 131-144.

21. Platania, C.B.M. and C. Bucolo, *Molecular Dynamics Simulation Techniques as Tools in Drug Discovery and Pharmacology: A Focus on Allosteric Drugs*, in *ALLOSTERY: Methods and Protocols*, L. DiPaola and A. Giuliani, Editors. 2021. p. 245-254.
22. Sedova, A., et al. *High-Performance Molecular Dynamics Simulation for Biological and Materials Sciences: Challenges of Performance Portability*. in *IEEE/ACM International Workshop on Performance, Portability and Productivity in HPC (P3HPC)*. 2018. Dallas, TX.
23. Zhao, L., et al., *Molecular Dynamics Simulations of Human Antimicrobial Peptide LL-37 in Model POPC and POPG Lipid Bilayers.* Int J Mol Sci, 2018. **19**(4).
24. Karplus, M. and J.A. McCammon, *Molecular dynamics simulations of biomolecules.* Nat Struct Biol, 2002. **9**(9): p. 646-52.
25. Guvench, O. and A.D. MacKerell, Jr., *Comparison of protein force fields for molecular dynamics simulations.* Methods Mol Biol, 2008. **443**: p. 63-88.
26. Vanommeslaeghe, K., et al., *CHARMM general force field: A force field for drug-like molecules compatible with the CHARMM all-atom additive biological force fields.* J Comput Chem, 2010. **31**(4): p. 671-90.
27. Mackerell, A.D., Jr., *Empirical force fields for biological macromolecules: overview and issues.* J Comput Chem, 2004. **25**(13): p. 1584-604.
28. Periole, X. and S.J. Marrink, *The Martini coarse-grained force field.* Methods Mol Biol, 2013. **924**: p. 533-65.
29. *C-QUARK: Contact Assisted Ab Initio Protein Structure Prediction*. Available from: https://zhanggroup.org/C-QUARK/.
30. *RCSB Protein Data Bank*. Available from: https://www.rcsb.org/.
31. Sato, H. and J.B. Feix, *Peptide-membrane interactions and mechanisms of membrane destruction by amphipathic alpha-helical antimicrobial peptides.* Biochim Biophys Acta, 2006. **1758**(9): p. 1245-56.
32. Mortuza, S.M., et al., *Improving fragment-based ab initio protein structure assembly using low-accuracy contact-map predictions.* Nat Commun, 2021. **12**(1): p. 5011.
33. Sun, M.A., et al., *Prediction of reversible disulfide based on features from local structural signatures.* BMC Genomics, 2017. **18**(1): p. 279.
34. Dombkowski, D.A. *Disulfide by Design v 2.13* Available from: http://cptweb.cpt.wayne.edu/DbD2/index.php)
35. Craig, D.B. and A.A. Dombkowski, *Disulfide by Design 2.0: a web-based tool for disulfide engineering in proteins.* BMC Bioinformatics, 2013. **14**: p. 346.
36. Gautier, R., et al., *HELIQUEST: a web server to screen sequences with specific alpha-helical properties.* Bioinformatics, 2008. **24**(18): p. 2101-2.
37. Abraham, M., et al., *GROMACS: High performance molecular simulations through multi-level parallelism from laptops to supercomputers.* SoftwareX, 2015. **1**.
38. *Bura, supercomputer at University of Rijeka*. Available from: https://cnrm.uniri.hr/hr/bura/.
39. Jo, S., et al., *CHARMM-GUI: a web-based graphical user interface for CHARMM.* J Comput Chem, 2008. **29**(11): p. 1859-65.
40. Lee, J., et al., *CHARMM-GUI Input Generator for NAMD, GROMACS, AMBER, OpenMM, and CHARMM/OpenMM Simulations Using the CHARMM36 Additive Force Field.* J Chem Theory Comput, 2016. **12**(1): p. 405-13.
41. Wu, E.L., et al., *CHARMM-GUI Membrane Builder toward realistic biological membrane simulations.* J Comput Chem, 2014. **35**(27): p. 1997-2004.
42. Jo, S., et al., *CHARMM-GUI Membrane Builder for mixed bilayers and its application to yeast membranes.* Biophys J, 2009. **97**(1): p. 50-8.

43. Huang, J., et al., *CHARMM36m: an improved force field for folded and intrinsically disordered proteins.* Nat Methods, 2017. **14**(1): p. 71-73.
44. Jorgensen, W., et al., *Comparison of Simple Potential Functions for Simulating Liquid Water.* J. Chem. Phys., 1983. **79**: p. 926-935.
45. Kern, N.R., et al., *CHARMM-GUI Multicomponent Assembler for Modeling and Simulation of Complex Multicomponent Systems.* bioRxiv, 2023: p. 2023.08.30.555590.
46. Murzyn, K., T. Róg, and M. Pasenkiewicz-Gierula, *Phosphatidylethanolamine-phosphatidylglycerol bilayer as a model of the inner bacterial membrane.* Biophys J, 2005. **88**(2): p. 1091-103.
47. Jo, S., T. Kim, and W. Im, *Automated builder and database of protein/membrane complexes for molecular dynamics simulations.* PLoS One, 2007. **2**(9): p. e880.
48. Parrinello, M. and A. Rahman, *Polymorphic transitions in single crystals: A new molecular dynamics method.* Journal of Applied Physics, 1981. **52**(12): p. 7182-7190.
49. Berendsen, H.J.C., et al., *Molecular dynamics with coupling to an external bath.* The Journal of Chemical Physics, 1984. **81**(8): p. 3684-3690.
50. Hess, B., et al., *LINCS: A linear constraint solver for molecular simulations.* Journal of Computational Chemistry, 1997. **18**(12): p. 1463-1472.
51. Essmann, U., et al., *A smooth particle mesh Ewald method.* The Journal of Chemical Physics, 1995. **103**(19): p. 8577-8593.
52. Reißer, S., et al., *3D hydrophobic moment vectors as a tool to characterize the surface polarity of amphiphilic peptides.* Biophys J, 2014. **106**(11): p. 2385-94.
53. Kabsch, W. and C. Sander, *Dictionary of protein secondary structure: Pattern recognition of hydrogen-bonded and geometrical features.* Biopolymers, 1983. **22**(12): p. 2577-2637.
54. *Gnuplot*. Available from: http://www.gnuplot.info/.
55. Turner, P., *XMGRACE, Version 5.1. 19.* Center for Coastal and Land-Margin Research, Oregon Graduate Institute of Science and Technology, Beaverton, OR, 2005. **2**.
56. Humphrey, W., A. Dalke, and K. Schulten, *VMD: visual molecular dynamics.* J Mol Graph, 1996. **14**(1): p. 33-8, 27-8.
57. Shinnar, A.E., K.L. Butler, and H.J. Park, *Cathelicidin family of antimicrobial peptides: proteolytic processing and protease resistance.* Bioorganic Chemistry, 2003. **31**(6): p. 425-436.
58. Li, J., et al., *Trypsin inhibitory loop is an excellent lead structure to design serine protease inhibitors and antimicrobial peptides.* The FASEB Journal, 2007. **21**(10): p. 2466-2473.

8 Appendix

8.1 Initial structures, systems, and simulation setup

Table 8.1 cQuark predicted models chosen as the initial structures in the simulations, with their C- and TM- scores.

Peptide	Model number	C - score	TM - score
TSO8(1-39)	3	-3.092	0.347 ± 0.143
TSO8(3-39)	2	-2.650	0.335 ± 0.137
TSO8_lin	1	-2.276	0.351 ± 0.144
TSO8(1-23)	1	-0.844	0.413 ± 0.140
TSO8(3-23)	1	-1.044	0.404 ± 0.144
TSO8(20-39)	5	-3.355	0.304 ± 0.115

Figure 41 Addition of the disulfide bridge to model 2 of TSO8(3-39) using Disulfide by design program.

Table 8.2 System size and properties for one peptide in water simulations.

Fragment	Water molecules	K^+ *ions*	Cl^- *ions*	Box dimensions (Å)
TSO8 (1-23)	14126	40	54	77 x 77 x 77
TSO8 (1-39)	14486	41	57	78 x 78 x 78
TSO8 (3-23)	15888	45	59	80 x 80 x 80
TSO8 (3-39)	14018	40	56	77 x 77 x 77
TSO8 (20-39)	9253	26	30	67 x 67 x 67
TSO8_lin	13470	38	54	76 x 76 x 76

Table 8.3 System size and properties for peptide with POPE:POPG membrane (P/L=1/256).

Fragment	Water molecules	K^+ *ions*	Cl^- *ions*	Box dimensions (Å)
TSO8 (1_23)	25138	117	67	87,343 x 87,343 x 147,283
TSO8 (1_39)	26388	118	70	87,343 x 87,343 x 152,373
TSO8 (3_23)	25035	117	67	87,343 x 87,343 x 146,956
TSO8 (3_39)	25998	117	69	87,343 x 87,343 x 150,942
TSO8 (20_39)	25162	127	67	87,343 x 87,343 x 147,132
TSO8 (lin)	26159	118	70	87,343 x 87,343 x 151,381

Table 8.4 Size and properties of systems containing several TSO8(1-39) peptides.

Number of peptides	**POPE:POPG**	**Water molecules**	K^+ **ions**	Cl^- **ions**	**Box dimensions Å**
6	**592**	71571	246	194	132,822 x 132,522 x 172,373
12	**592**	69910	194	238	132,822 x 132,522 x 172,373
12	**-**	19031	53	245	86,90 x 86,90 x 86,90

Table 8.5 Equilibration steps for peptide with membrane simulations.

Step	**Ensamble**	**Time step dt (fs)**	**Duration (ps)**	**Force constant** $kcal/(mol\text{Å}^2)$			
				Position restraints			**Dihedral restraints**
				Backbone	**Side chains**	**P atoms**	
1	NVT	1	125	10.0	5.0	2.5	2.5
2	NVT	1	125	5.0	2.5	1.0	1.0
3	NpT	1	125	2.5	1.3	1.0	0.5
4	NpT	2	500	1.3	0.5	0.5	0.5
5	NpT	2	500	0.5	0.1	0.1	0.3
6	NpT	2	500	0.1	0.0	0.0	0.0

8.2 Problems with creating larger systems

While creating the system containing multiple peptides in the vicinity of the membrane, one could encounter a few problems. First, it is important to choose a large enough membrane system, to more reliably represent the interaction of the peptides with the membrane. Secondly, number of water molecules added to the system is crucial. If the thickness of the water layer above the peptides is not large enough, peptides could move vertically and leave the simulation box, and end up on the other side of the membrane, which, for our model, would mean that they have entered the cell. Those results must be discarded. This was the case for the simulation of twelve peptides in the vicinity of the membrane, described in section 5.3.2, where one peptide vertically moved away from the membrane after 700 ns, leading to uninterpretable results.

However, adding a very thick water layer results in extreme simulation times, so it is crucial to determine the water molecule per lipid ratio for the system to yield results in the reasonable time.

Another issue can occur when using supercomputers. For the simulation of twelve peptides, several systems were constructed each leading to different challenges. The first selected membrane model contained 512 lipids and a 4 nm water layer thickness, which proved to be insufficient, as peptides swiftly left the simulation box. Another attempt was with a membrane of 768 lipids, and a 4 nm water layer, which on the other hand resulted in a very long simulation time, and the peptides still moved vertically out of the box. The number of lipids was then reduced to 672, with an 8 nm water thickness, and this system exhibited problems while trying to run a simulation at the supercomputer, due to decomposition issues. On a traditional computer, which uses a different type of parallelization compared to the supercomputer, the simulation was able to run, but predicted an unreasonably long time for computing.

The final system size was determined mostly by trial and error but keeping in mind that the water to lipid ratio should be around 100.

8.3 Additional results

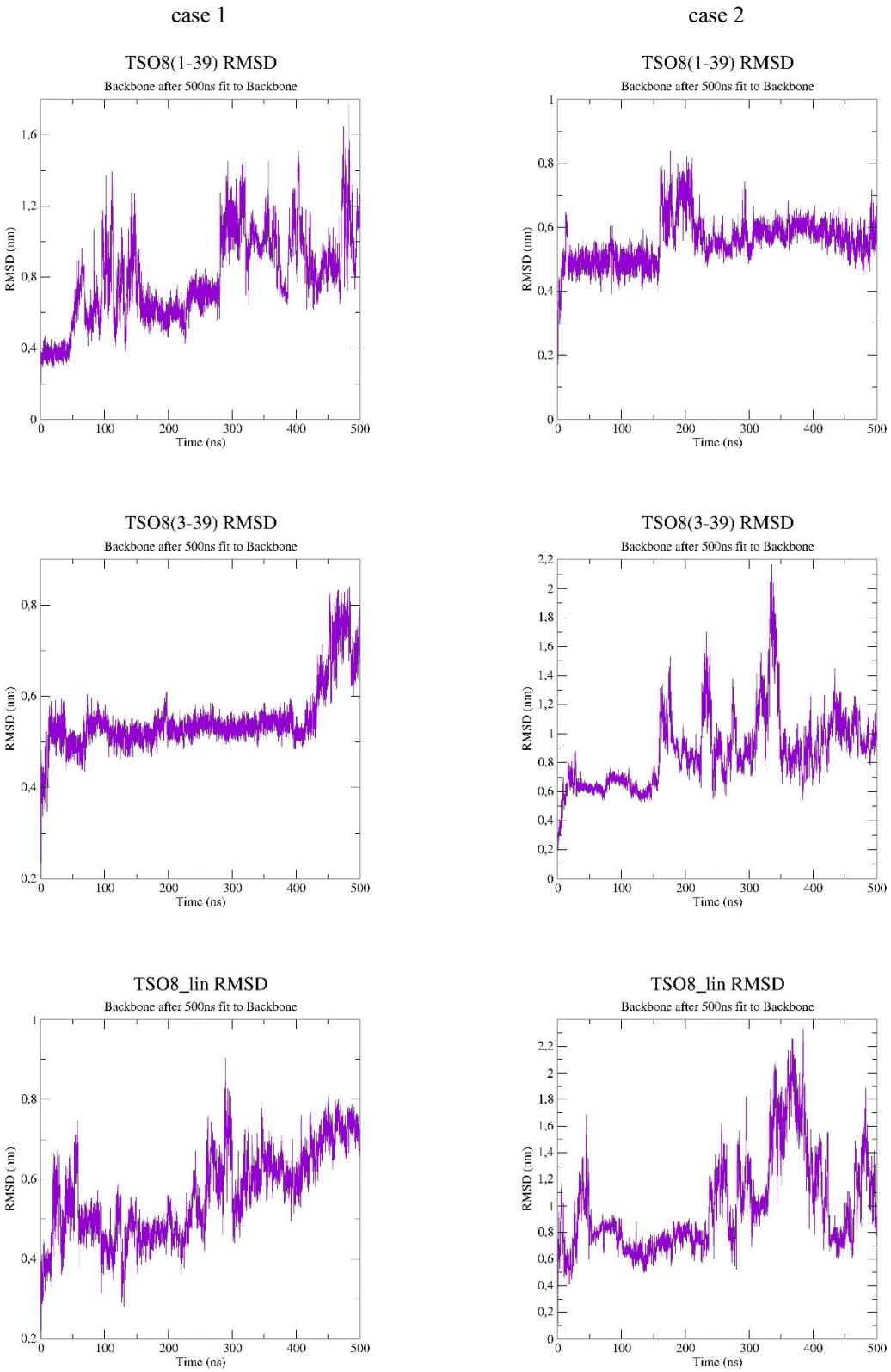

Figure 42 RMSD calculations for two cases of 500 ns long simulations of TSO8(1-39), TSO8(3-39) and TSO8_lin in water.

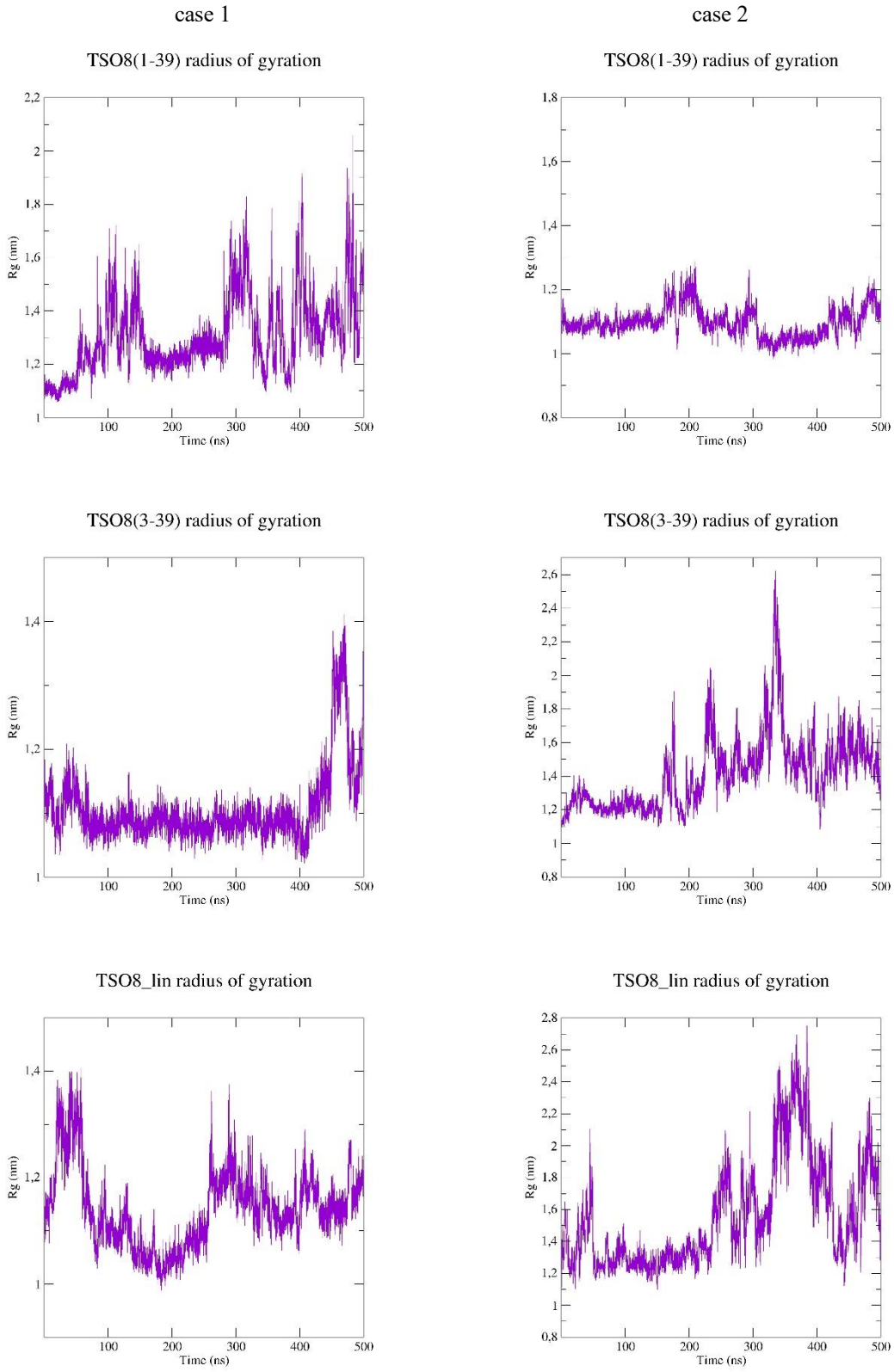

Figure 43 Radius of gyration calculations for two cases of 500 ns long simulations of TSO8(1-39), TSO8(3-39) and TSO8_lin in water.

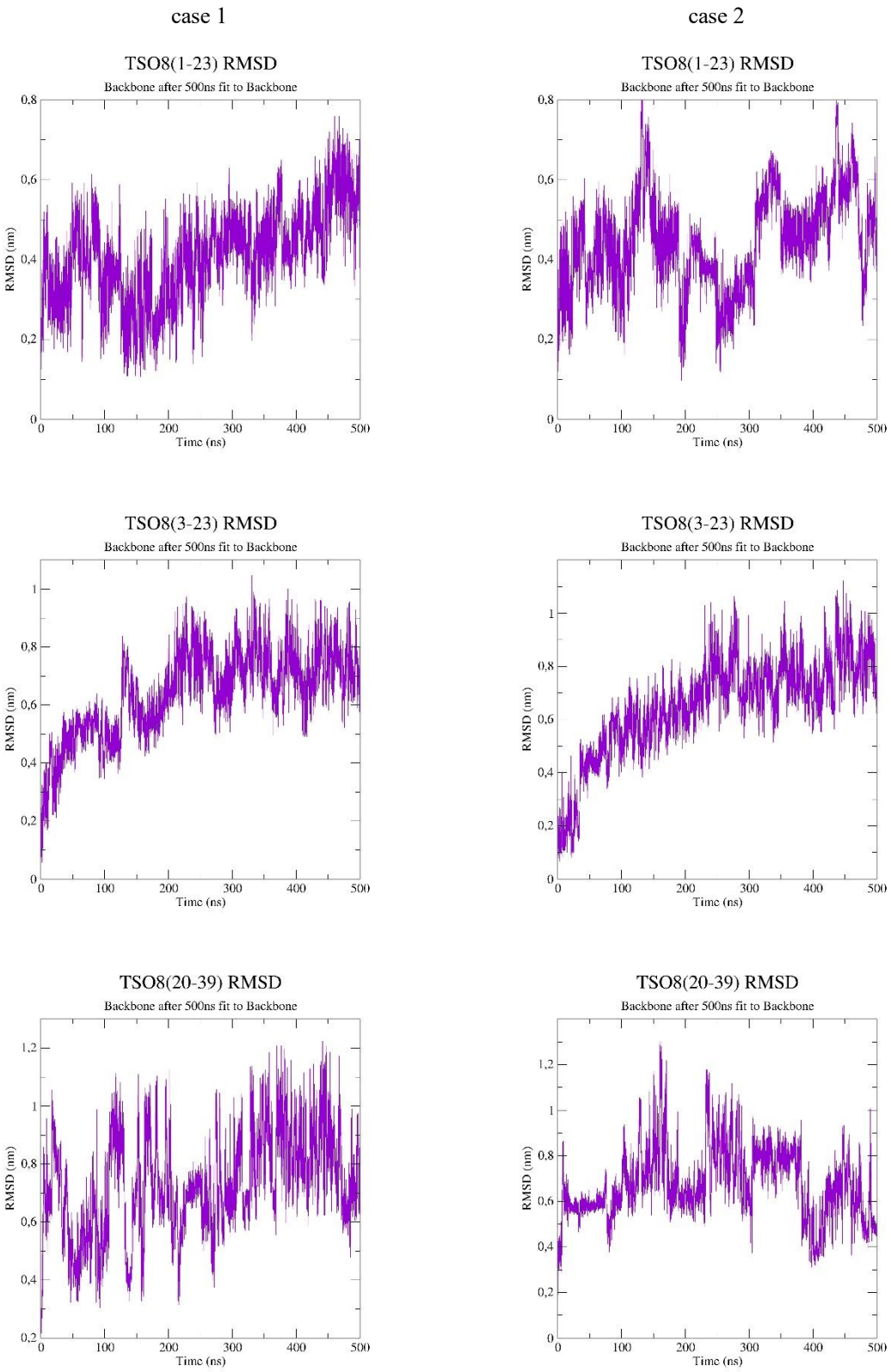

Figure 44 RMSD calculations for two cases of 500 ns long simulations of TSO8(1-23), TSO8(3-23) and TSO8(20-39) in water.

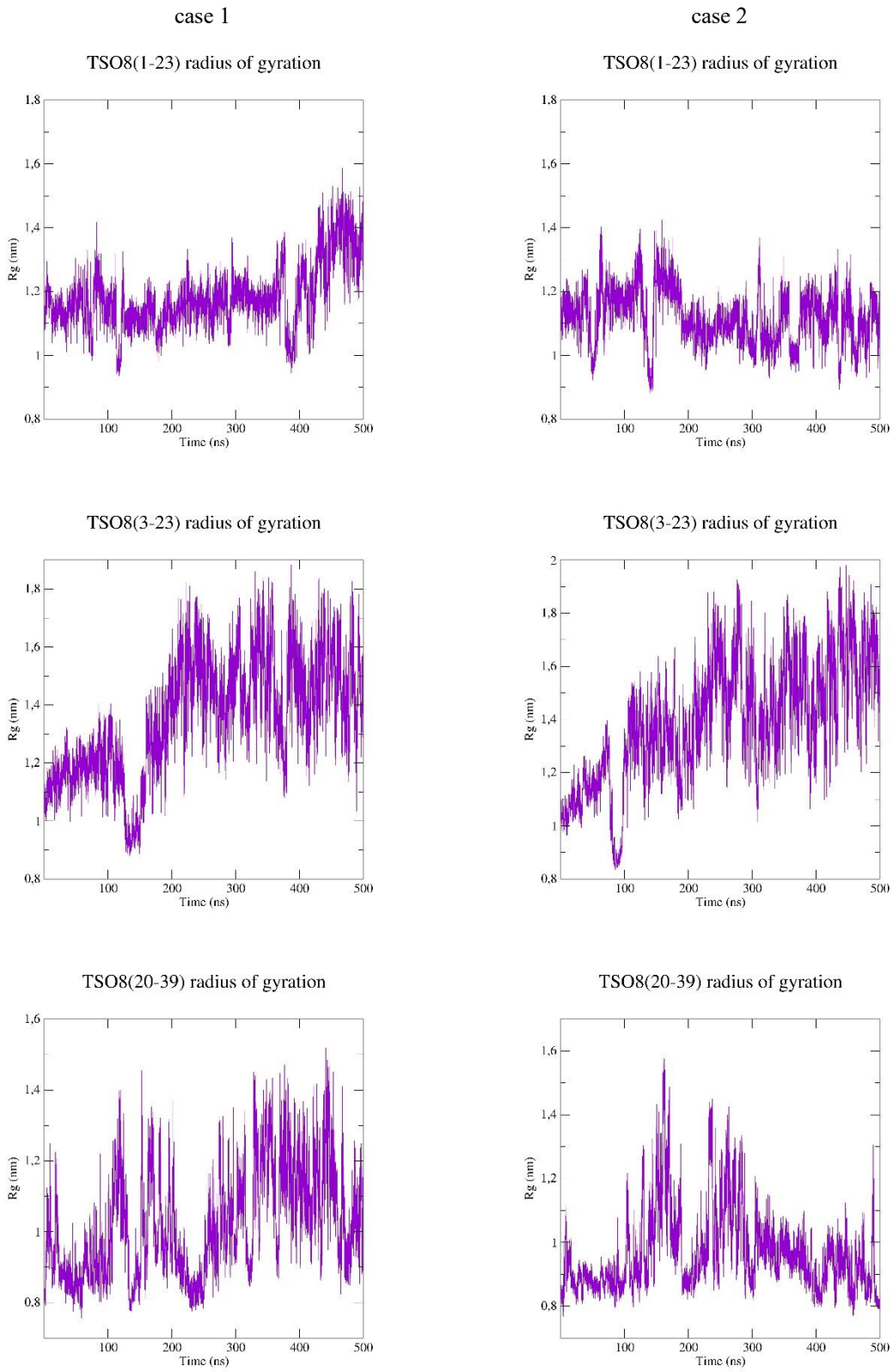

Figure 45 Radius of gyration calculations for two cases of 500 ns long simulations of TSO8(1-23), TSO8(3-23) and TSO8(20-39) in water.

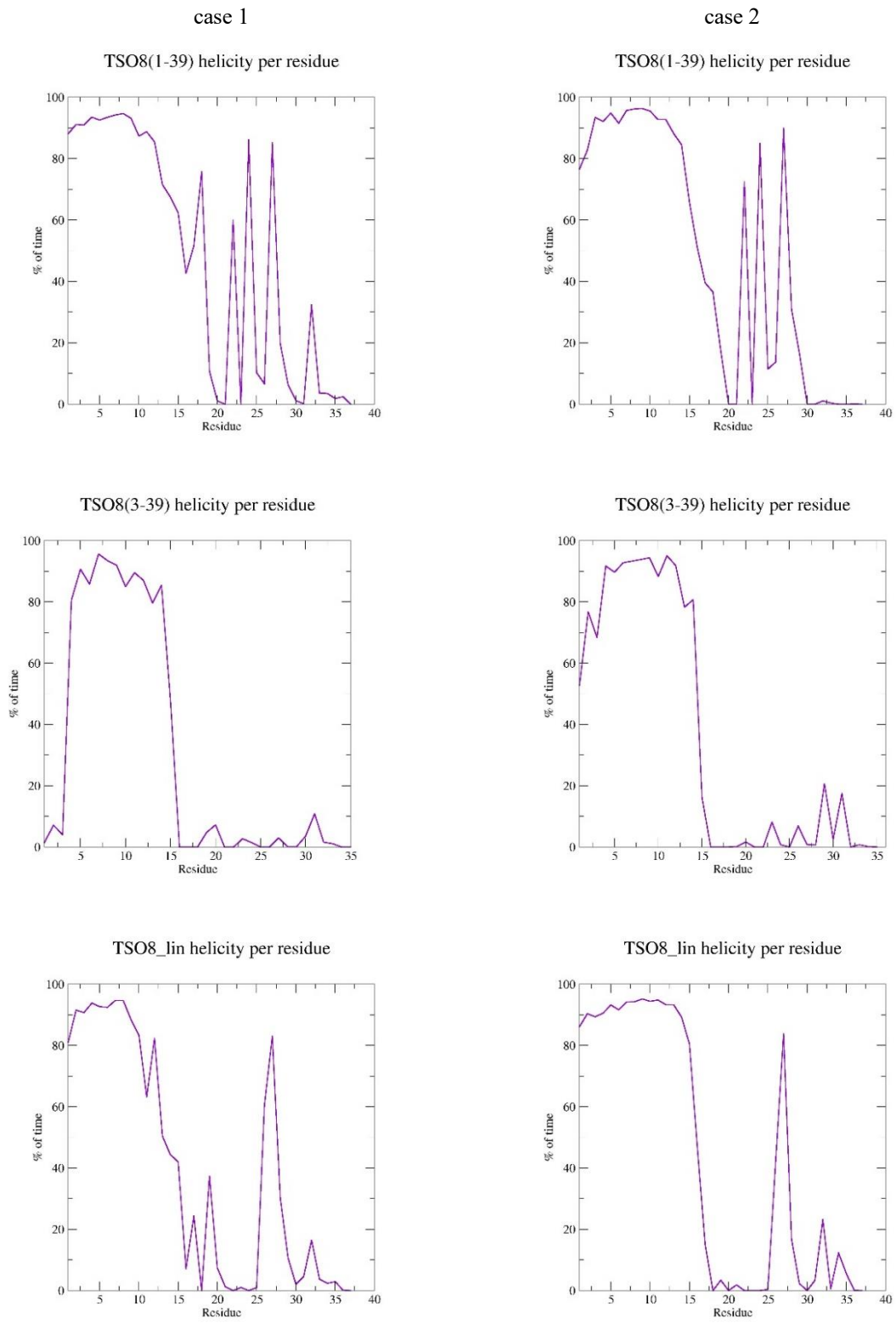

Figure 46 Helicity per residue calculated for TSO8(1-39), TSO8(3-39) and TSO8_lin during two cases of 500 ns simulations in water.

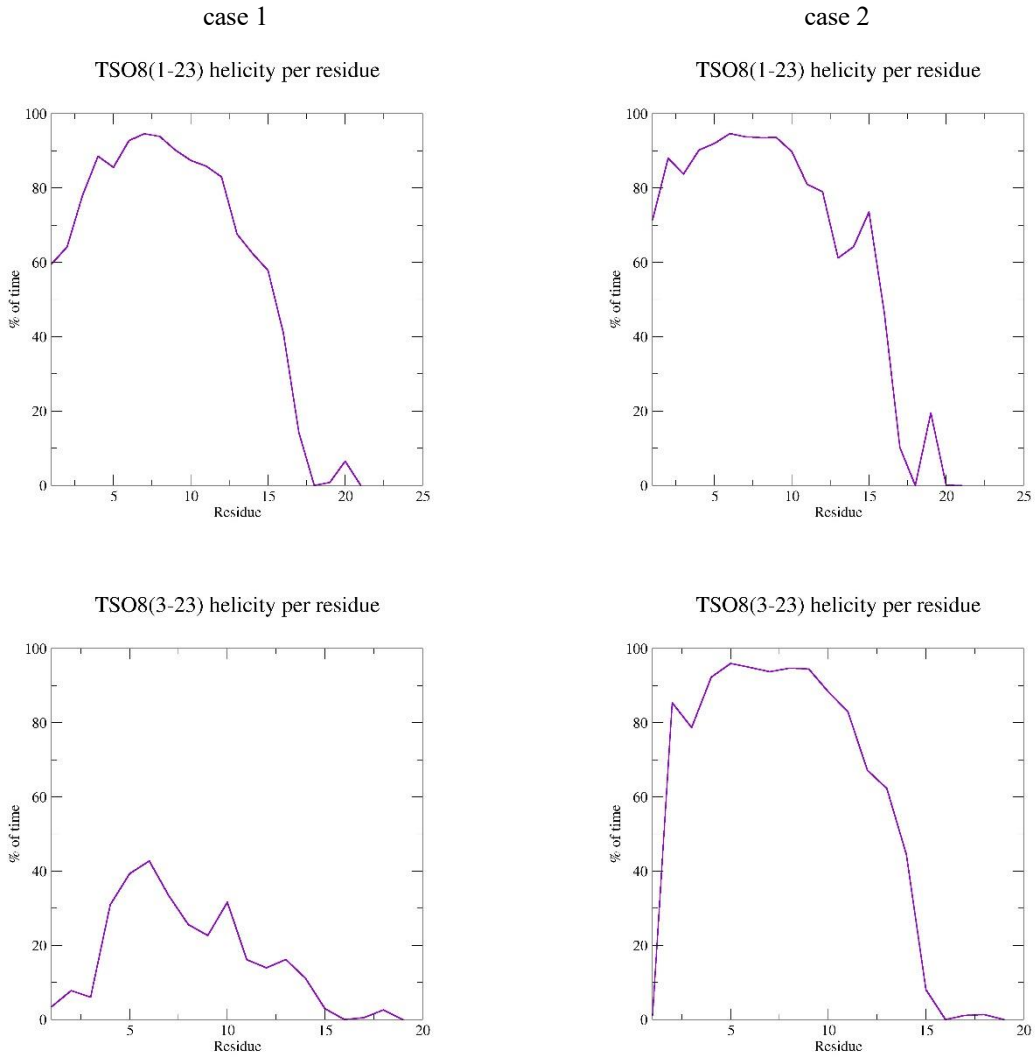

Figure 47 Helicity per residue calculated for TSO8(1-23) and TSO8(3-23) during the 500 ns simulation in water (left) and 1.0 μs simulation with the membrane (right)

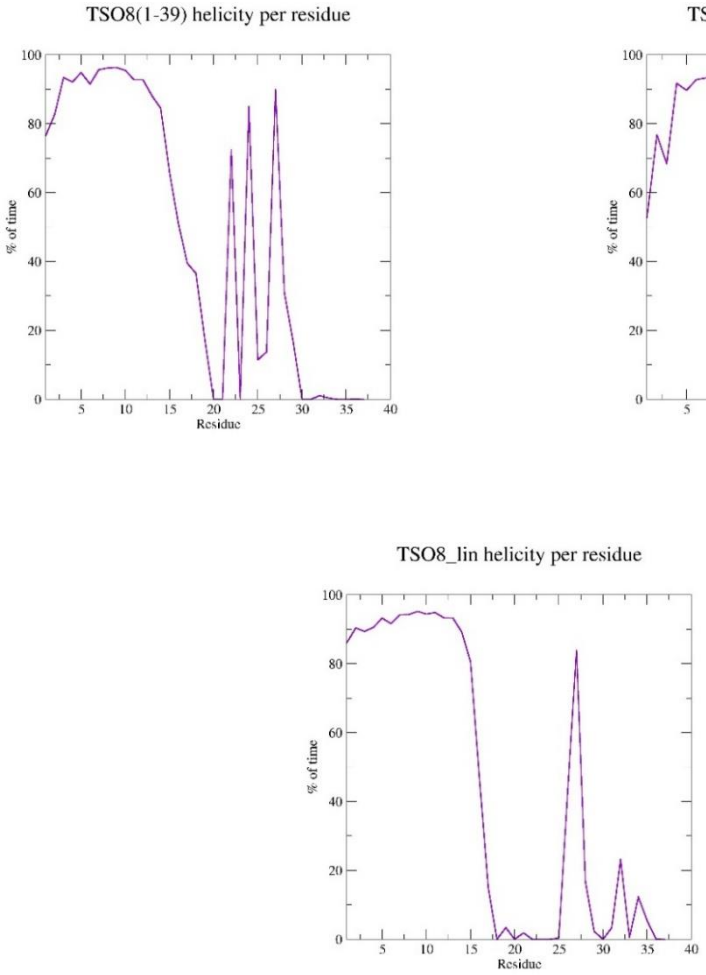

Figure 48 Helicity per residue calculated for TSO8(1-39), TSO8(3-39) and TSO8_lin during the 1.5 μs simulation in the vicinity of the membrane.

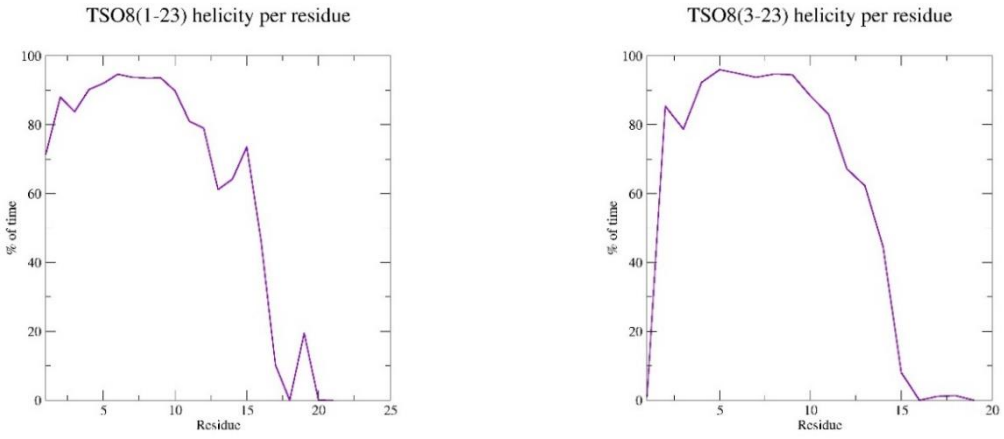

Figure 49 Helicity per residue calculated for TSO8(1-23) and TSO8(3-23) during the 1.0 μs simulation in the vicinity of the membrane.

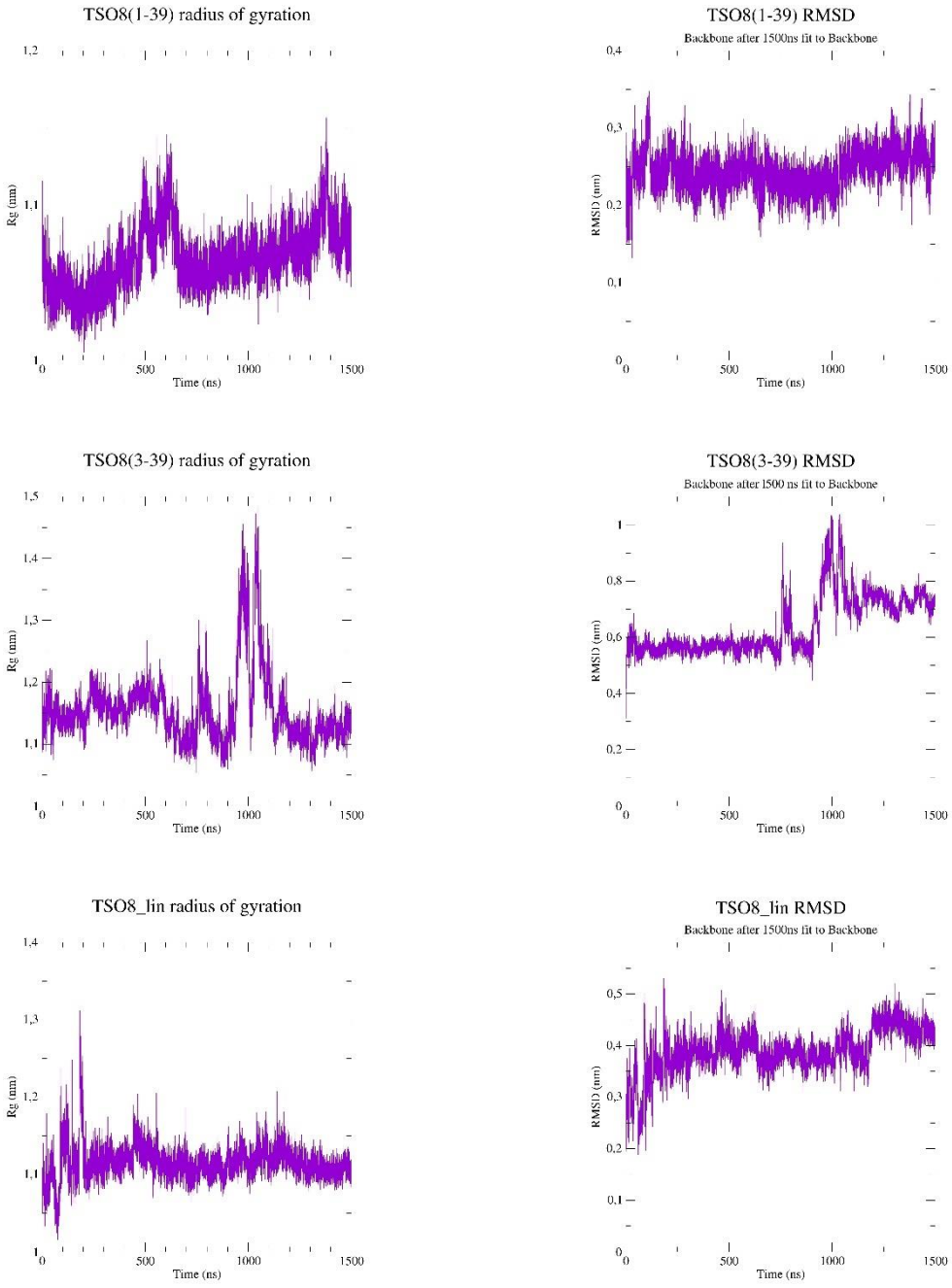

Figure 50 Radius of gyration (left) and RMDS (right) calculated for TSO8(1-39), TSO8(3-39) and TSO8_lin during the 1.5 μs simulations with the membrane.

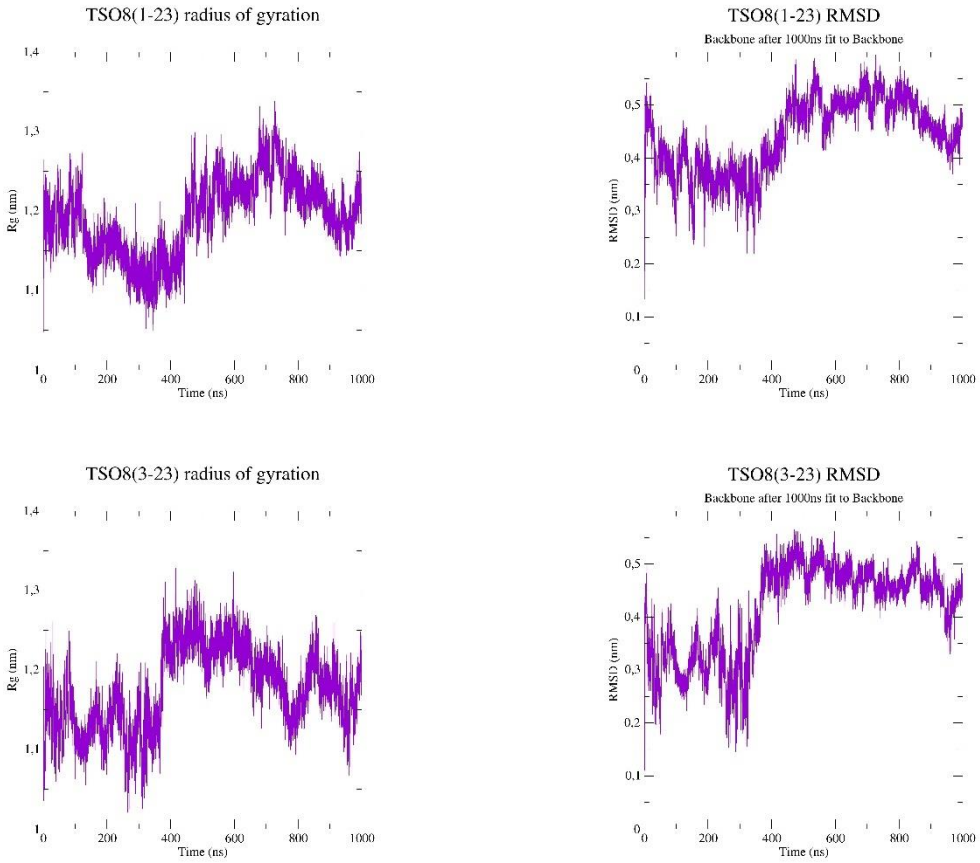

Figure 51 Radius of gyration (left) and RMDS (right) calculated for TSO8(1-23) and TSO8(3-23) during the 1.0 μs simulations with the membrane.